Modeling of Human Color Vision System

Anahit Pogosova

Master's thesis
Department of Computer Science and Statistics
University of Joensuu

Modeling of Human Color Vision System

Anahit Pogosova

Department of Computer Science and Statistics
P.O. Box 111, FI-80101 Joensuu, FINLAND.

Master's thesis

Abstract

The aim of this work is to study human color vision system. For that purpose some of the existing models of human color vision were implemented and examined. Previously they have mainly been applied to grayscale or RGB images, which brings discrepancy with real visual system even before the model processing. One of the key approaches in this study is the use of spectral color information, instead of traditional 3-dimensional color representations. In this work different ways of applying color vision models to spectral images are considered. The emphasis is placed on the two well-known models: vector model by Ingling & Tsou (1977) and the Retinex theory for color computation by Land (1964). Some of the experiments, performed with these models are also described.

This work is a part of an ongoing cooperation between the University of Joensuu, University of Kuopio and Lappeenranta University of Technology. Within the limits of this study only the models, having physiological and psychophysical basis are considered. One of the goals of the study is to create a general color vision model in an n-dimensional spectral space.

Key words:
Color vision models, Retinex, color appearance, spectral images.

Acknowledgments

This thesis is the conclusion and the result of my participation to the IMPIT program at the department of Computer Science and Statistics at the University of Joensuu. It has been two unforgettable years, for which I would like to express my deep gratitude to Professor Jussi Parkkinen, Dean of the Faculty of Science at the University of Joensuu, who gave me the opportunity to participate to this program and to complete my Masters degree in Finland. Moreover, he further kindly agreed to be my supervisor. I want to thank him for his grate patience and understanding, for his valuable advises and optimism, without which this work would not be possible.

I would like to express my sincere appreciation to Professor Tiimo Jääskeläinen, Head of Department of Physics at the University of Joensuu, who was the reviewer of my thesis. Thank you for the time you have spent on reading my work and for your thoughtful comments.

The work on this thesis was carried out within the Color Research Group at the University of Joensuu. The warm and encouraging atmosphere within the group made this an unforgettable and rewarding experience. I would like to express my particularly heartfelt gratitude to Tuija Jetsu. She was the first person to whom I directed all my questions and was always ready to help and discuss on any matter. Moreover, she had kindly agreed to be the first person to read my thesis and gave extremely valuable and precise comments. I can not overestimate her role in this work, for which I express my deepest gratitude. I also want to thank Markku Hauta-Kasari, Director of the InFotonics Center at the University of Joensuu, for his infectious enthusiasm, endless optimism, and support.

Many people have helped and supported me during my stay in Joensuu. In particular, I want to express my gratitude to Merja Hyttinen and Wilhelmiina Hämäläinen for their assistance, valuable advises and constant and warm support that they have shown through my stay in Joensuu.

In particular, I want to thank all my friends, especially Alina and my dear Yuri. They where always there for me, and were the first readers and critics of my work. Thank you for the inspiration and patience.

And finally, I want to express my deepest appreciation and gratitude to my family. Without your love, help, support, and deep believe in my abilities I would have never made it.

Contents

List of Notations

A	Achromatic
CIE	Commission Internationale de l'Eclairage
D	Deuteranopic
GC	Gain Control
LGN	Lateral Geniculate Nucleus
R, G, B	Red, Green, Blue
RG	Red-Green
T	Tritanopic
YB	Yellow-Blue

LMS	long-, medium-, short-wavelength sensitive cone responses
r-g	red-green opponent channel
y-b	yellow-blue opponent channel
V_λ	luminance achromatic channel

λ	wavelength in nanometers
$I(\lambda)$	radiance value at wavelength λ
$I^x(\lambda)$	radiance value at wavelength λ for a pixel x

Chapter 1

Introduction

Our visual system is as elaborate and complex, as important in our everyday life. The studies have shown that we get approximately 80% of all external information through our vision. Within the human visual system, *color vision* has its special place. It helps to recognize and distinguish surrounding objects based on their colors, which we characterize to be bright or dull, saturated or not, red, green, purple, etc. We easily agree on those characteristics of color usually without any notion about their bases and physical meanings. Most of us take color vision for granted and do not know much about the complex mechanisms and pathways behind it.

Still, understanding the underlying principles and mechanisms of human color vision is often essential. Although there are yet numerous gaps in our knowledge about visual system, there is still a large interest towards it. There are various applications where characteristics of human vision are important, such as painting, image and video processing and compression, machine and robot vision. Medical application is the other aspect.

In many of those examples an adequate *mathematical model of human color vision* is required. For example, in the case of medicine, such a model will help to study the behavior of the visual system in various conditions and situations, to predict possible deficiencies and vision restrictions. These, in turn, can open new ways for vision deficiency treatment.

Before attempting to create a proper model of human color vision, it is necessary to get acquainted with already existing ones. Nowadays several such models of color vision exist, e.g. [IT77], [Gut91], [DVDV93], [LM71]. They are aimed to serve different functions and demonstrate different performance. Most of such models are using traditional 3-dimensional color spaces. Unlike that, the starting point in this

study is in n-dimensional *spectral data* and images. *Spectral reflectance* is a very accurate, device and illumination independent representation of the color signal. By using spectral data, we are able to visualize accurately, for example, the effect of light source changes in images [JHP+07].

This work is restricted to the consideration of already existing color vision models having physiological and psychophysical bases. Different ways of applying color vision models to the n-dimensional spectral data are proposed and their behavior and performance are examined.

The separate issue of this work is the evaluation of the color vision models. Several evaluation methods or the modifications of the existing ones are proposed in order to evaluate the spectral approach.

In general, this work is a part of an ongoing study. One of its objectives is to understand color vision at general level and to develop a mathematical, n-dimensional vector space model for describing the essential properties of human color vision.

This work is organized as follows. Chapter 2 provides the necessary overview of the fields of color and vision. Here some physical aspects of color are introduced first. Color is described as a specific property of an object. Later in this chapter the biological properties of the human visual system are described. Here we see how the visual system processes the received color signal.

Chapter 3 provides a review of the mechanisms and properties of human color vision. Here the two essential theories of color vision are described: *trichromatic theory* and *opponent color theory*. The causes of several vision phenomena are clarified and their importance in the attempts to model human color vision is emphasized. The chapter also tells about several color representation systems. Here we see that spectral images provide most accurate color information.

Chapters 4 and 5 concentrate on the color vision models. In Chapter 4 four well-known models are described in details and some of their differences and peculiarities are emphasized. The last section of this chapter is dedicated to the Retinex model, which was the central subject of this study. Chapter 5 represents the implementation and evaluation of two of the described models: the Ingling & Tsou vector model [IT77] and the Retinex model for lightness computation [LM71]. Here the proposed approaches for the model evaluation are described and the obtained results are summarized. We see that the spectral approach, in some way, justifies the expectations.

Finally, the work is summarized in Chapter 6. Some additional issues of possible improvements are addressed.

Chapter 2

Color and Vision

Color of an object can be considered as one of the physical properties of the object, along with, for example, its weight, size or shape. However, it differs from all other physical properties. To perceive (or measure) color of an object it must be exposed to *light* and, unlike all of the other physical properties, color can be judged through no other sense than *vision* (while we can, for example, estimate the weight or the size by looking at the object or by touching it). To summarize, color of an object is a property which can be perceived by an observer[1] through his vision only when there is an interaction with light. But it exists even when there is nobody around to perceive it [KB96].

In this chapter some basic aspects of color and human visual system are introduced. These will help to understand some underlying principles behind the complicated process of color perception. Sections trough 1 to 3 describe some physical properties of light and color, while the remaining sections are concentrated on the human visual system.

2.1 Light and color

Even far back in the past people (ancient Greeks) believed that we can see an object because something passes between the object and our eye. Today we can state,

[1] Further we will concentrate only on the visual system of a human observer. Considering animal vision (as well as mechanical vision) can be an issue for a separate research and is out of scope of this work. We also will use "he" when talking about an abstract person. This by no means is intended to exalt or depreciate any of the genders.

that "something", coming to an eye and stimulating the visual perception is *light*, modulated by the surface of the object and reflected to the eye.

Light is a form of electromagnetic radiation. Further, when talking about light, we mean light which can be perceived by a human eye. It forms a narrow part of the electromagnetic spectrum from approximately 380 to 780 nanometers (1 nanometer is 10^{-9} meter) and is referred to as *visible light*. Corresponding spectrum is called a *visible spectrum*. Figure 2.1 illustrates how narrow the visible spectrum is.

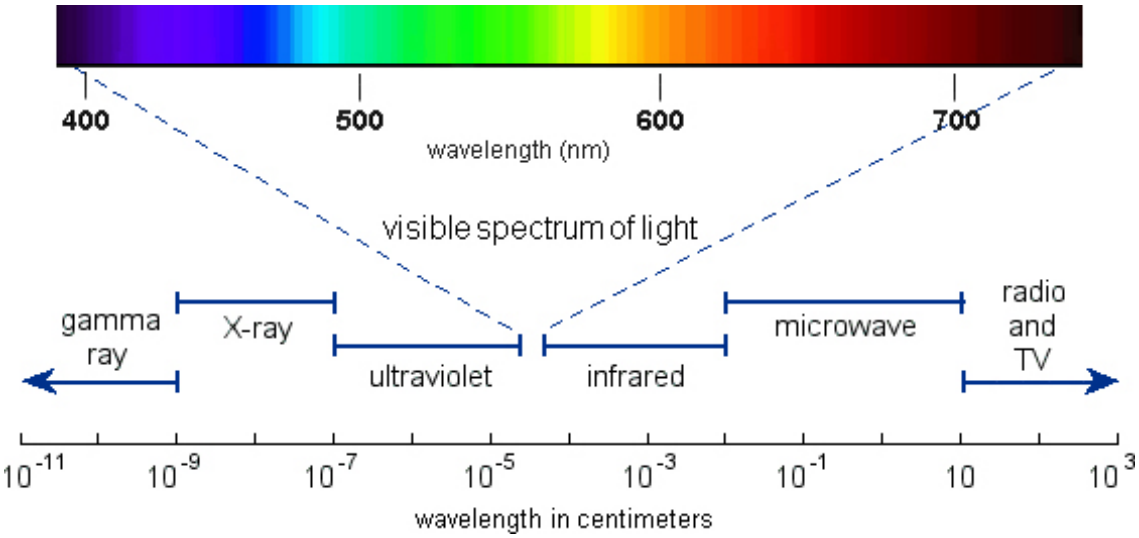

Figure 2.1: The visible spectrum in the total spectrum of electromagnetic energy.

One of the fundamental concepts behind the theory of electromagnetic radiation is the so-called *wave-particle duality*. It implies that light, which is a wave by its nature, also behaves as a flux of particles. These particles of light are called *photons*. Photon is an indivisible unit of radiant energy, which has a zero rest mass. As it also possesses wave properties, we associate its energy E with its wavelength λ and velocity of light c by the following formula:

$$E = \frac{hc}{\lambda}, \tag{2.1}$$

where $h = 6,62 \times 10^{-34}$ is the *Planck's Constant*.

The brighter light is the more photons it contains. When there are enough photons (high intensity), there exists a correspondence between the wavelength of light

and its hue, perceived by an observer. Light consisting of a single wavelength is *monochromatic light*, which looks to the eye as a *pure color*. The shortest perceptible wavelengths of the visible spectrum appear violet (bellow which is the *ultraviolet* region), while the longest visible wavelengths appear nearly pure red (after which it is the *infrared* region) (see Fig. 2.1). The table below represents the six pure spectral colors and approximate wavelength intervals associated with them, proposed by Le Grand in 1957 [LG57]:

Color	**Wavelength interval (nm)**
Violet	$\sim$ 400–440
Blue	$\sim$ 440–500
Green	$\sim$ 500–570
Yellow	$\sim$ 570–590
Orange	$\sim$ 590–610
Red	$\sim$ 610–700

Table 2.1: Spectral colors and associated approximate wavelength intervals.

Sir Isaac Newton was not the first person to split the white light into spectrum with the help of a prism (around 1665-1666), but he was the first to state, that it is not the prism that colors light. He stated [New72]:

> "For the Rays to speak properly are not coloured. In them there is nothing else than a certain Power and Disposition to strip up a Sensation of this or that Colour."

The results of Newton's experiments can be considered among the most important results through the history of color science.

2.2 Sources of light

There are various sources of radiant energy. Some of them are natural, while others are artificial. Among the natural sources of light, *sun* is the most important one for the human eye. It emits energy of various wavelengths, some of them too short or too long to see. Before reaching the human eye, the distribution of the wavelengths is significantly altered by the earth's atmosphere (see Fig. 2.2). The artificial light occurs usually when something is burned or heated to a required temperature, e.g. the filament in an incandescent lamp or a candle.

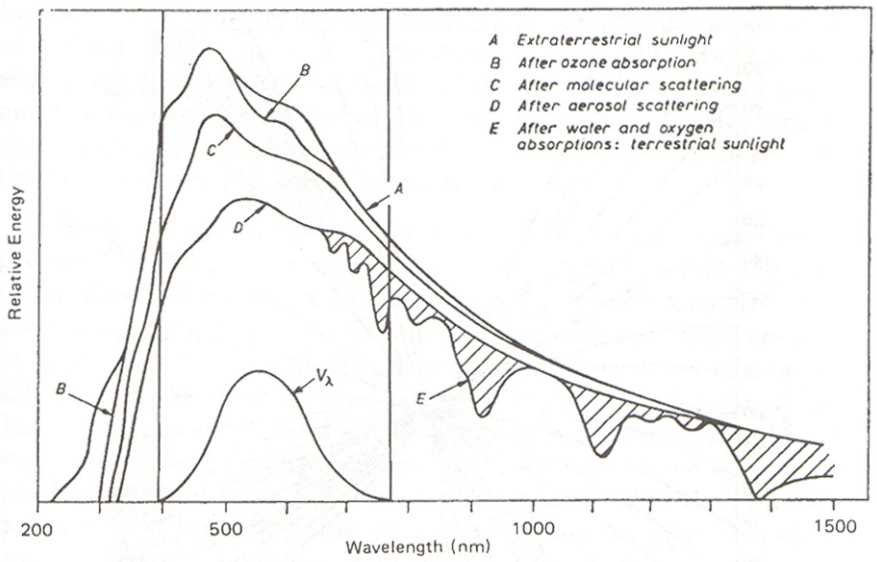

Figure 2.2: Spectral distribution of sunlight before and after entering the Earth's atmosphere (scanned from [KB96], p. 67).

The light sources differ in their *spectral power distribution* - the relative amount of energy at each wavelength. As it was stated, we are interested in the wavelengths within the visible spectrum. The International Commission on Illumination (*Commission Internationale de l'Eclairage*, or *CIE*) has published several standardized tables of spectral power distribution values called *standard illuminants*. Some of them represent existing light sources, while others are statistical approximations. Among the standard illuminants is the illuminant A representing an incandescent light source, and illuminants $D50$ and $D65$, which are statistical representations of average daylight with color temperature[2] about 5000K and 6500K, respectively (see Fig. 2.3). CIE also introduced the illuminants B and C, which were intended to represent direct sunlight and average daylight, respectively. However they were later considered inadequate and the $D50$ and $D65$ illuminants are being widely used instead [WS00].

[2]Color temperature of the illuminant is the temperature at which the heated black-body radiator emits light of the same (or nearly the same) color as the illuminant.

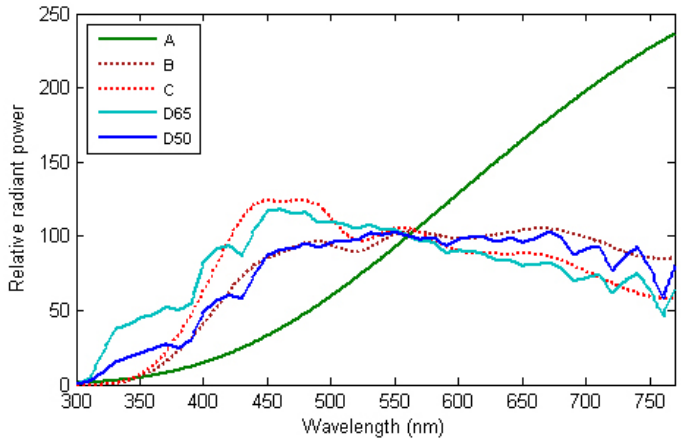

Figure 2.3: Spectral power distribution of 5 standard illuminants: A, B, C, $D65$ and $D50$.

2.3 Light and objects

Perceived color of an object highly depends on the light source and on the properties of visual system (this will be discussed in details in the following sections). But even more important is how light interacts with the object.

Light has a tendency to move in straight lines until it encounters a medium, different from that it has been traveling through. Here several things may happen (see Fig. 2.4). Light can be *refracted* by the medium and then *transmitted* through it (if the medium is transparent), or *absorbed* by it (transforming into heat). It can be *scattered* inside the medium if the medium is not completely transparent (is other than vacuum) because of the collision of photons with the molecules of the medium (like sunlight scattering in the atmosphere). And finally, light can be *reflected* from the surface of the medium. The reflection of light is crucial in color perception.

Color of an (opaque) object can be characterized by the *spectral reflectance* of the object: the distribution of wavelengths of light, reflected from its surface. The spectral reflectance of the object describes an object just as the spectral power distribution describes a light source.

The color signal reaching the eye when observer focuses on an object is the signal from the light source, modulated by the surface of the object. To describe the amount of light reaching the eye from a particular area of an object we use *radiance* values. For each wavelength λ_n, the radiance equals to the product of the spectral power distribution of the ambient light and the surface reflectance:

$$I^x(\lambda_n) = S^x(\lambda_n)E(\lambda_n), \tag{2.2}$$

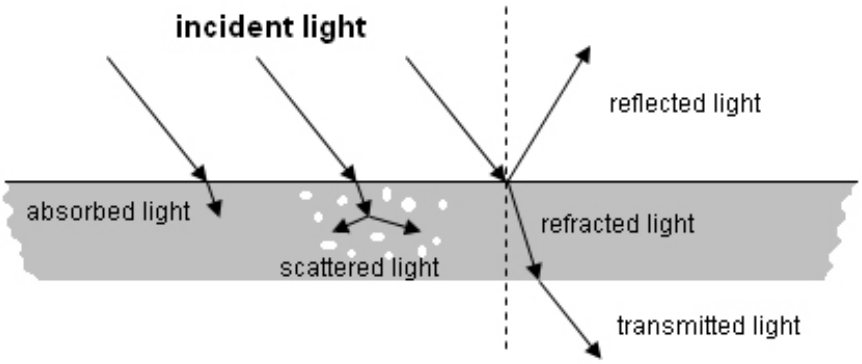

Figure 2.4: Different ways in which light interacts with encountered medium.

where $I^x(\lambda_n)$ are the radiance values for pixel x, $S^x(\lambda_n)$ are the surface reflectance values and $E(\lambda_n)$ is the spectral power distribution of the ambient light.

2.4 The eye

The *eye* is a part of the mechanism by which humans see colors. Understanding its functions is crucial in the attempts to model color vision. In this section the main structure of the human eye is shortly described (Fig. 2.5). More detailed information on this subject, as well as on the subjects of remaining sections, can be found, for example, in [KB96], [Rob02], [Fai98], or on the web [KFN].

Cornea and Sclera

Light entering the eye first passes through the *cornea* - the transparent outer surface at the front of the eye (see Fig. 2.5). Cornea is the part of the eye with the biggest refractive power. This means, that cornea is responsible for eye focusing and image forming. This is achieved due to its form (cornea can be imagined as a lens with both faces curved in the same direction) and its index of refraction (it significantly differs from the refraction index of the air outside the eye, and is almost the same as the refractive indexes of other bodies inside the eye).

The most important property of the cornea is that it is highly transparent. Cornea transmits almost all of the light in the visible part of the electromagnetic spectrum, while absorbing in the ultraviolet part, which helps to prevent the damage of other components of the eye.

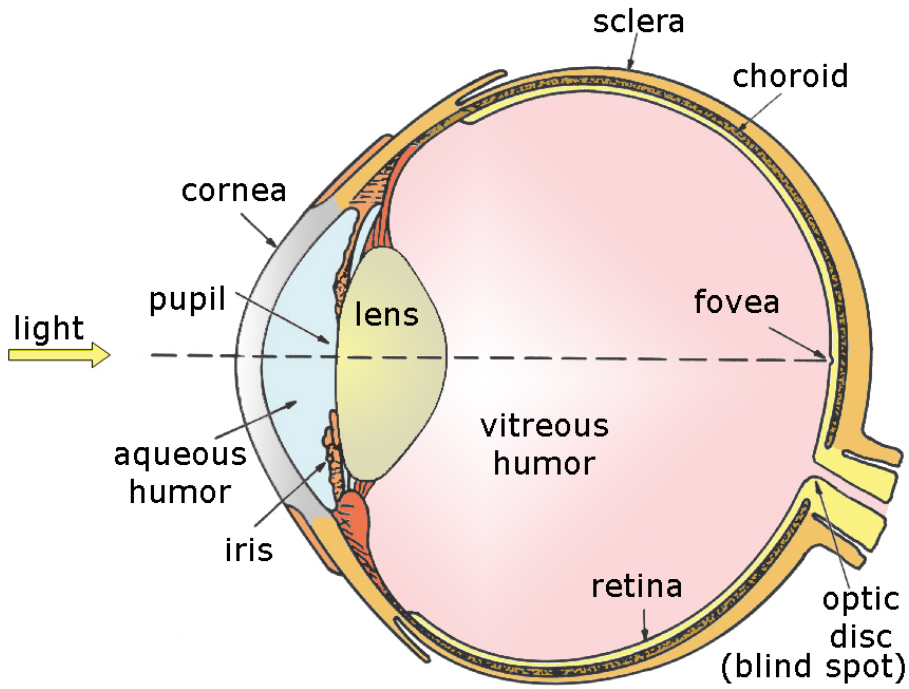

Figure 2.5: Schematic diagram of the human eye.

Protection of the eye from injuries and outer damages is an important function of the cornea. It is able to stand the difference in pressure inside and outside the eye and is richly endowed with the pain receptors to inform the brain about the risks of possible injuries.

Sclera, or "the white of the eye", constitutes the outer protective layer of the eye and is contiguous with the cornea.

Lens

Along with the cornea, *lens* participates in the process of focusing. However, unlike the cornea, its curvature is not fixed, but can be changed according to the conditions. When focusing on nearby objects, lens becomes "fatter", while when focusing on distant objects, it becomes "flatter". This is controlled by the ciliary muscles.

Lens serves also as a short-wavelength filter, protecting the eye from the harmful short wavelength energy. As we age, lens looses its ability to change in shape, which makes it impossible to focus on the nearby objects. Also, with age, lens starts to absorb more and more short-wavelength light (becomes more yellow), which influences color vision.

Humors

The space between the cornea and the lens is filled with the *aqueous humor*. It is exceptionally clear and has an affinity for water. The *vitreous humor* fills about two-thirds of the eye (space between the lens and retina) and has a higher viscosity than the aqueous humor being partly a gel and partly a liquid.

The humor inside the eye is of a slightly higher pressure than that of the atmosphere. This helps to preserve the shape of the eye and to make it more resistant to the outer damages.

Iris and pupil

Iris is the pigmented part of the eye, which determines the "color of the eyes". It contains muscles that control the amount of light, passing through to the retina, by changing the size of the *pupil*. The pupil is the circular opening in the center of the iris. It is contracted or dilated by the muscles of the iris with the changes in the illumination (when the illumination is dim, the pupil is dilated, while when the illumination is bright, the pupil is contracted). However, illumination is not the only factor on which the size of the pupil depends. One of the factors is the emotional state, which does not necessarily have something to do with vision.

The pupils of both eyes change in size simultaneously, even if light is delivered to only one eye. These changes are initiated by the same photoreceptors that mediate vision.

2.5 The retina

The *retina* serves for light detection, transition of electromagnetic energy to the neural signals and initial processing of the signals, before they are transmitted further to the brain. All this functions are carried out by the neural cells which form the retina.

The retina is extended against the back of the eye (Fig. 2.5) adjacent to the *retinal pigment epithelium* and *choroid*, layers of the eye that provide oxygen and nourishment to the outer layers of the retina (see Fig. 2.6). They also absorb the light that happens to not be absorbed by the photoreceptors or that passes through the sclera. This prevents chromatic aberration and provides sharpness and contrast of the perceived image.

Although the human retina contains about 200 million nerve cells, it is less than a millimeter thick over most of its extent [KB96]. The retina is composed of *photoreceptor* layer, which is connected to the *ganglion cells* through a series of layers of neurons. The axons of ganglion cells are the *optic nerve* fibers, connecting retina to the *lateral geniculate nucleus* (LGN), unit of the brain, processing visual information (more details on the brain visual pathways are described in the following sections). The optic nerve, composed of about 1 million axons ([Rob02]) leaves the eye through the *optic disc*, or *blind spot* (Fig. 2.5). In general, the retina is a part of the central nervous system and can be appropriately considered to be a part of the brain.

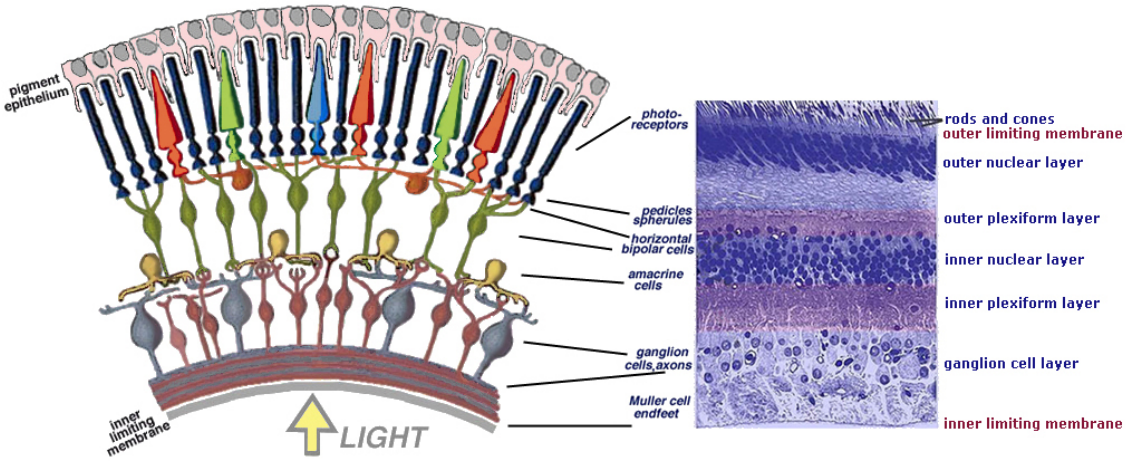

Figure 2.6: Schematic diagram of the cross-section of the retina (on the left) with the micrograph of a vertical section through central retina (adopted from [KFN]).

2.5.1 Photoreceptors

The most of the light photons entering the eye end up by being absorbed by the photoreceptors. Here the electromagnetic energy is transferred to nerve signal which, after the following processing by the neurons of the retina, is transmitted forward to the brain for visual perception.

The photoreceptor layer is situated at the back of the retina (Fig. 2.6). There are two classes of photoreceptors: *rods* and *cones*. Their names originally came from their shapes: cylindrical and conical, respectively (see Fig. 2.7). However in some areas of the retina the cones are so tightly packed that they became more cylindrical and similar to rods (see p. 16). There are still some structural differences between the rods and the cones. One of them is the difference in the synaptic

terminals (Fig. 2.7). The termination of the rod is called the *spherule* and is of a spherical form. Cones, on the other hand, terminate with the *pedicle* which is foot-like in appearance. Both rods and cones have indentations at their base, called *invaginations*. A single cone pedicle contains several invaginations, while a rode spherule has only one invagination. Through the cone pedicles, rod spherules and their invaginations the connection of the photoreceptors to the further layer of the neural cells takes place.

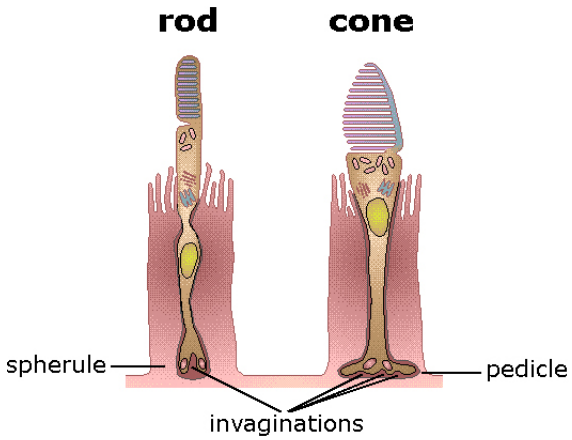

Figure 2.7: Illustration of the photoreceptors: rods (on the left) and cones (on the right), surrounded by the outer limiting membrane (adopted from http://www.colour4free.org.uk).

Still, the difference in shape is not the main distinction between the two classes of photoreceptors. It is the difference in their functional and photochemical properties that is of great importance.

Rods are highly sensitive and function only under low illumination conditions. They serve for the achromatic night (*scotopic*) vision. Cones, on the contrary, serve for the day (*photopic*) vision under the higher illumination conditions and are responsible for acute and color vision. There is also a case (e.g. around dawn), when both rods and cones are functioning simultaneously. This kind of vision is called *mesopic* vision. Differences in the photoreceptors give the visual system the ability to function over twelve orders of magnitude of light intensity, from dim starlight to the bright sunlight [Rob02]. More details about the contribution of the photoreceptors to the color vision are described in the following chapter.

As the photoreceptor layer is situated at the back of the retina (Fig. 2.6), light must pass through all the other layers of neural cells before it reaches the photoreceptors. Location of the photoreceptors allows them to get enough nutrients and easily process the waste products [Fai98].

2.5.2 Neural layers

The retina consists of three layers of neural cells: the *outer nuclear layer*, the *inner nuclear layer* and the *ganglion cell layer* (Fig. 2.6). The outer nuclear layer consists of the cell bodies of the photoreceptors, described above; the inner nuclear layer includes bodies of the *horizontal cells*, *bipolar cells*, and most of the *amacrine cells*; the last layer of the retina is composed of the cell bodies of the *ganglion cells* and displaced amacrine cells. Between the nucleus layers are the two layers of linking synapses: the *inner plexiform layer* and the *outer plexiform layer*. The retina is restricted by the *outer* and *inner limiting membranes* (see Fig. 2.6).

The retina also contains so-called *Müller cells*, which are glia cells that spread from the outer to the inner limiting membrane. Müller cells support the structure of the retina. The other functions of Müller cells are not completely understood yet [KB96].

The pathways from the outer nuclear layer to the inner nuclear layer can be divided to the *direct* and *lateral* pathways. The direct pathway connects photoreceptor cells with ganglion cells through the bipolar cells. The lateral pathway includes also horizontal and amacrine cells. Rod photoreceptors can also connect directly to a specific class of ganglion cells [Rob02].

Horizontal cells

Horizontal cells spread laterally across the retina in the inner nuclear layer. The dendrites and axons of horizontal cells make connections in the outer plexiform layer. The two major types of horizontal cells are the so-called *H1* and *H2* cells. They differ in the type of the photoreceptors they connect to. The dendrites of H1 cells connect cones, while their axons connect rods only. The dendrites and axons of H2 cells contact only cones.

It is suggested that each cone connects with two to four horizontal cells. Each horizontal cell, in its turn, is believed to have seven terminals each connecting to a different cone [Rob02].

There are several suggestions about the functions of the horizontal cells. Some suggest, that they modulate the signal from cones to bipolar cells, others suggest that they influence the potentials of photoreceptors themselves. In any case, horizontal cells appear to join groups of photoreceptors [KB96].

Bipolar cells

Bipolar cells, like horizontal cells, are also spread in the inner nuclear layer, while their dendrites lie in the outer plexiform layer. However, unlike horizontal cells, the axons of bipolar cells make connections in the inner plexiform layer and the cells act to deliver signals from the photoreceptors to ganglion cells. Bipolar cells differ in the spread of their dendrites (*midget* and *diffuse bipolars*) and in the type of their connection to the photoreceptors (*flat bipolars* and *invaginating bipolars*). There is a separate class of bipolar cells, connecting only to rods.

A midget bipolar cell appears to be chromatically selective and its dendrites connect to a single cone. A diffuse bipolar cell is not chromatically selective and serves luminance type function, connecting with several cones. In the peripheral retina diffuse bipolars can contact with from 5 up to 14 cones and more [Rob02]. Both, midget and diffuse cells can be flat or invaginating. Flat cells connect to the base of cone pedicles, while invaginating cells contact with the invaginations in the terminations of the photoreceptors.

Amacrine cells

The last in the inner nuclear layer are amacrine cells (although sometimes amacrine cells can be found in the ganglion cell layer as well). They, like horizontal cells, are spread laterally. However, amacrine cells mostly lack axons (the name "amacrine" means "... a cell lacking a long process (axon)" [KB96]) and make their connections in the inner plexiform layer with bipolar and ganglion cells. Amacrine cells are probably responsible for motion detection.

Ganglion cells

The innermost layer of the retina, the ganglion cell layer, consists (mostly) of the ganglion cell bodies. Ganglion cells can be classified according to the structure of their dendrites to two major classes: *midget* and *parasol* ganglion cells. Midget ganglions receive their input from a small number of midget bipolar cells. They are probably involved in high acuity and color vision. Parasol ganglion cells receive their input from diffuse bipolar cells. They are probably involved in achromatic, low spatial vision, and movement and luminance detection [Rob02].

The axons of ganglion cells make up the optic nerve, which leaves the eye through the optic disc and heads for the LGN. The part of the retina where the optic nerve leaves the eye naturally does not contain any photoreceptors to detect light. Thus,

a part of a visual scene is not perceived (it is then filled by the brain with the surrounding information or the information from the other eye). This area on the retina is thus called *the blind spot* (see Fig. 2.5).

2.5.3 The fovea and the peripheral retina

There is a small pit in the central part of the retina, where it is less than half as thick as anywhere else across the eye. It is situated approximately on the visual axes and is called the *fovea*, or the *fovea centralis* (Fig. 2.5). It is the part of the retina, responsible for acute (color) vision and for providing fine visual details. When focusing on an object, eye moves in such way, that light from the object falls on the fovea.

The fovea is situated in the *macula* region, containing screening pigments, which act like short-wave filters. This, together with the cornea and lens, protects the fovea from the possible damages, caused by the ultraviolet energy, and helps to reduce chromatic aberration.

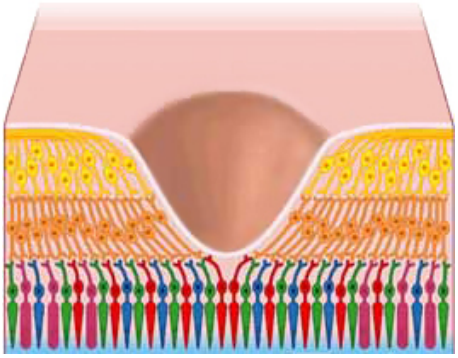

Figure 2.8: Schematic representation of the fovea centralis (adopted from www.brainconnection.com).

In order to provide acute color vision, the central fovea is packed with cone photoreceptors and does not contain any rods at all (Fig. 2.9). Cones are so tightly packed here, that they are more slim, elongated and rod-like than anywhere else across the retina. Moreover, to prevent light scattering in the central fovea, all the layers of neural cells (including the cell bodies of the cones themselves) are laterally displaced and are packed around the rim of the fovea, making it the thickest part of the retina (Fig. 2.8). Finally, there are no blood vessels in the central fovea, as they are not transparent and can cast shadows on the photoreceptors [KB96].

The outer plexiform layer, consisting mainly of the dendrites of ganglion cells, is much thicker around the fovea than across the remaining retina. This is partly because of the high number of cone photoreceptors, and partly because of the number of ganglion cells, connecting with each cone in the fovea centralis. The later is one of the parts of the mechanism in the fovea, providing acute color vision. Each cone from the central fovea connects with 3-4 ganglion cells. This ratio decreases to one ganglion cell per cone at an eccentricity of 3-4 mm and in peripheral retina there are more cones than ganglion cells [WGRB90].

As it can be seen from Figure 2.9, rods and cones are spread non-uniformly across the retina. The number of cones significantly decreases outside the fovea, while the number of rods increases. In general, the number of photoreceptors through the retina varies among the observers. However in the human retina there are significantly more rods (more than 95% percents of all photoreceptors in the human eye) than cones [GS99].

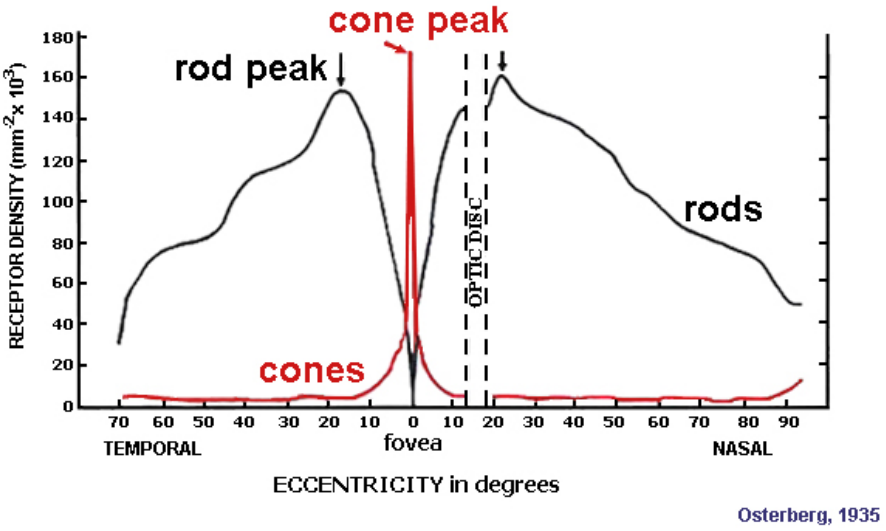

Figure 2.9: Rod and cone density as a function of retinal location (from [KFN]).

2.6 Visual pathways

The optic nerve leaves the eye at the optic disc, carrying the gathered visual information further, to the part of the brain, called *lateral geniculate nucleus*, or *LGN*. There are two lateral geniculate nuclei, one lies in the left hemisphere of the brain, and the other in the right hemisphere. The left LGN is responsible for processing the

information from the right side of the visual field, and the right LGN is responsible for the information from the left side of the visual field.

The LGN represents a layered structure, composed of six layers (see Fig. 2.10). Layers 1 and 2 contain large cells, named *magnocellular* (M) cells, which receive their signals directly from parasol ganglion cells and thus, probably, do not process chromatic information. Layers from 3 to 6 contain small cells, called *parvocellular* (P) cells, connecting with the axons of midget ganglion cells. Those are the layers of the LGN, which are probably responsible for processing of chromatic information and mediating color vision.

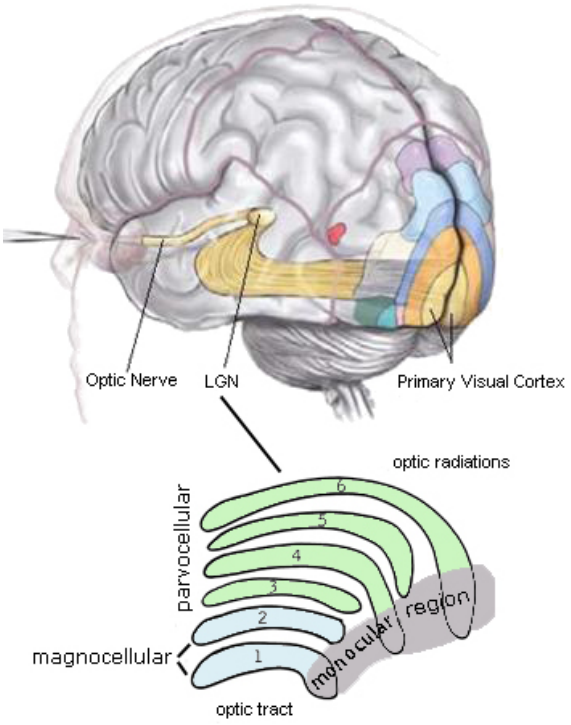

Figure 2.10: Picture of the brain showing the primary visual cortex, the lateral geniculate nucleus (LGN), and the optic nerve and schematic representation of LGN layers (partly adopted from http://scien.stanford.edu).

The axons of the cells of the LGN carry the processed visual information to the destination point in the brain: *primary visual cortex*. There is, probably, also a feedback system, through which some signals are sent back to the LGN and from there even to the retina. However, those systems are not appropriately studied yet, and, along with the further details about the functions of LGN and visual cortex, as well as with details about the corresponding pathways, are too complex and are

beyond the scope of this work. More information on this and related subjects can be found in corresponding literature, e.g. [Rob02], [GS99] and [KFN]. Figure 2.11 represented below illustrates the complexity of the visual pathways. It shows all the currently known areas within the macaque monkey visual pathway. The visual system of macaques is known to be similar to that of humans. The boxes in the figure represent the areas, and the lines represent the known neural connections between all the visual areas. The labels in the boxes refer to specific areas in the brain, which need not to be described here ([Rob02]).

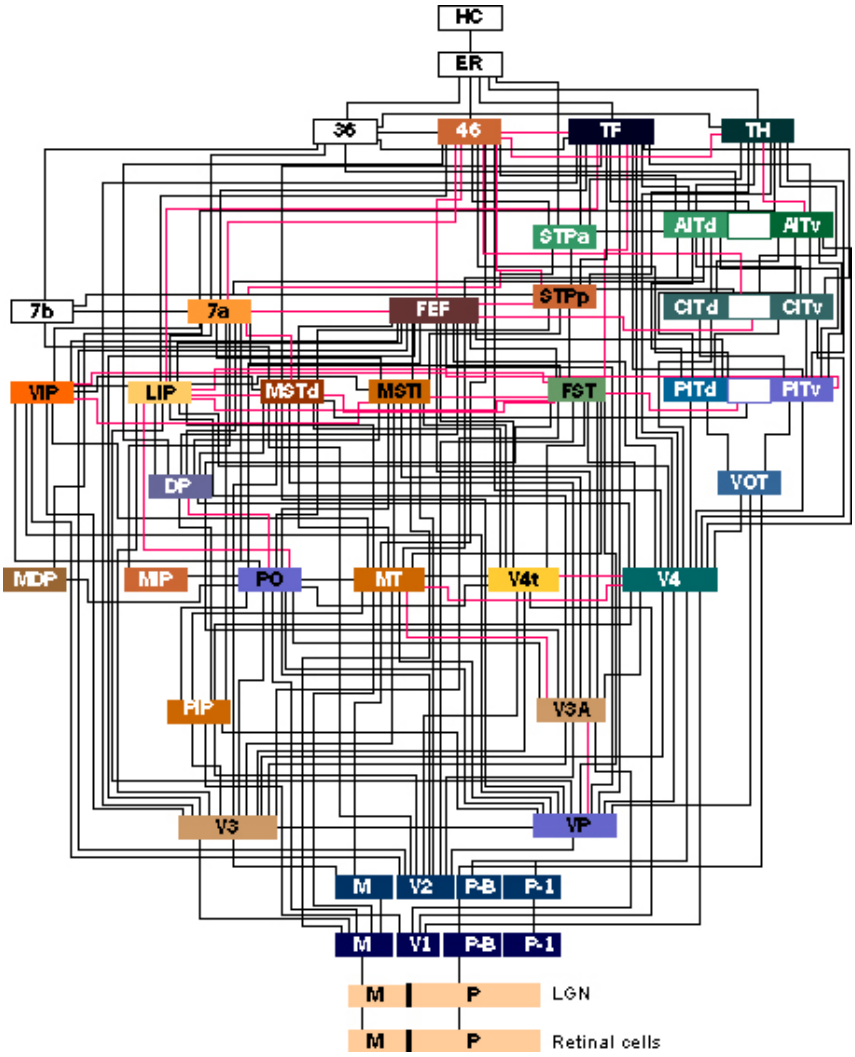

Figure 2.11: Macaque monkey visual pathways (adopted from http://www.wellesley.edu/Chemistry/Chem101/brain/brain.htm and [Rob02], p.164).

Chapter 3

Color Vision

As one can see from the previous chapter, human visual system is an extremely complex mechanism, which is not completely understood yet. However, some of its properties and mechanisms are already analyzed and must be considered in the attempts to create a valid artificial model of human color vision. The first stage of every model, claiming to have biological bases, is supposed to imitate the absorption of the color signal by the photoreceptors. On the following stages the outputs of all photoreceptors are to be combined to form three separate channels, transferred further to the brain, rather than transferring the outputs of separate photoreceptors. There are also some mechanisms, such as *adaptation*, which must be taken into account, as they underlie many of the color appearance phenomena, e.g. *color constancy*. Finally, in some cases it is appropriate to consider special cases of different types of color deficiencies.

In this chapter some of the main mechanisms and properties of human color vision are described. Two fundamental theories of color vision are introduced: trichromatic theory and opponent color theory, along with some color appearance phenomena. In addition, in the end of the chapter, several color representation systems are introduced. Some of them are based on the properties of visual system and will be used in the later chapters of this work.

3.1 Trichromatic color vision

The first fundamental theory of color vision being introduced is called *theory of trichromatic color vision*. It was suggested based on the psychophysical observations, long before it became possible to reveal the underlying physiological principles.

However, the trichromatic color vision theory remains, perhaps, the most essential mechanisms of human color vision system.

The retina of an individual with normal color vision (see the section "Color vision deficiencies" on the page 26 for description of "reduced" color vision) contains two types of photoreceptors, rods and cones, as it was already described in the previous chapter. The photoreceptors differ in the properties of light sensitive photopigments, residing at the outer segments of rods and cones. When the photopigment absorbs a photon of light, it undergoes some chemical transformations, which initiate a complex process leading to visual sensation.

The pigment inside a rod photoreceptor is called *rhodopsin*. This pigment absorbs light at very low intensities and thus, makes vision under low illumination conditions (e.g. at night) possible. The probability, that rhodopsin will absorb a single light photon differs for different wavelengths. This dependence can be illustrated with the *spectral sensitivity* (or, in the case of an isolated photopigment, the *spectral absorption*) curve (see Fig. 3.1). However, once a photopigment molecule absorbs a photon of light, the information about its wavelength is lost. This means, that an absorbed photon at, for example, 400 nm will cause the same sequence of actions as an absorbed photon at 600 nm, although, the photon at smaller wavelength possesses more energy (see Formula (2.1)). More simply, a photoreceptor is essentially a sophisticated photon counter, which makes a single-variable response to the incoming light according to the amount of photons it absorbed [GS99, Rob02]. This is a fundamental property behind the photopigments (and corresponding photoreceptors) and it is called the *principle of univariance*. The principle of univariance is the reason, why night vision is achromatic: a single photoreceptor type (rod) does not provide any information about the spectral composition of the light it has absorbed.

Unlike rod photoreceptors, there are three different types of cones. They differ in the photopigments they posses, which, in turn, differ in their spectral sensitivities to light of different wavelengths. This is the base for color properties of the visual system. The three classes of cones have their peak sensitivities at approximately 420 nm (short-wavelength sensitive cones, or *S cones*), 530 nm (medium-wavelength sensitive cones, or *M cones*) and 560 nm (long-wavelength sensitive cone, or *L cones*) (spectral absorption curves are represented in Fig. 3.1(a)). However, the cone sensitivities, when measured in a live human eye (not isolated), are slightly different (see Fig. 3.1(b)). There is a shift towards the longer wavelengths, caused by the influence of lens and macula (in the case of foveal cones), which absorb most of the short-wavelength energy.

Additional details about the behavior of spectral sensitivity curves can be seen, when the spectral sensitivities are represented in the logarithmic scale, as in Figure

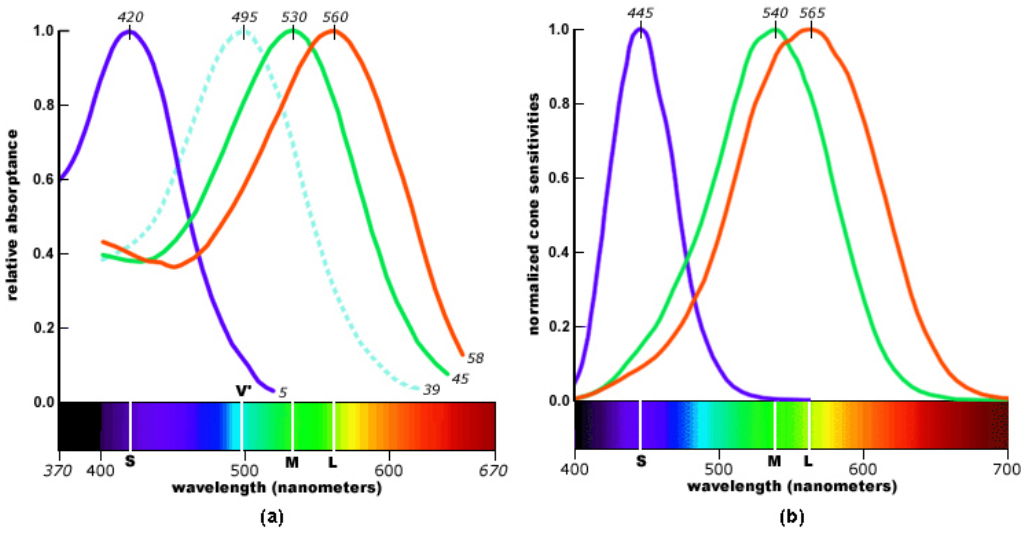

Figure 3.1: (a) Spectral absorption curves measured with the isolated photoreceptors; number of photoreceptors measured for each curve is at base of each curve; data from Dartnall, Bowmaker & Mollon (1983); (b) Spectral sensitivity curves, measured inside the eye, taking into account lens and macula effect on the transmitted light signal; based on the Stockman & Sharpe (2000) 10° quantal cone fundamentals. All curves are normalized to unity peak height (adopted from http://www.handprint.com/HP/WCL/color1.html).

3.2. From both representations of cone spectral sensitivities one can see, that the curves largely overlap (especially the curves of L and M cones). Thus, light never stimulates just one cone type. It has to stimulate either all three of them, or, at least, two of them. This means, that each color that we see is a combination of responses of several cone types. We never see a pure output of a single cone type.

The cone processing is the first stage of color vision. The *responses* of L, M and S cones to the light signal with known wavelength distribution can be estimated using spectral sensitivity curves of the corresponding photoreceptors (Fig. 3.1). The light signal reaching the eye can be described by radiance values $I(\lambda_n)$ for each visible wavelength λ_n (see Formula (2.2)). Thus, the formula for computation of cone responses ρ_k can be given as follows:

$$\rho_k = \sum_{n=1}^{N} C_k(\lambda_n) I(\lambda_n), \tag{3.1}$$

where $C_k(\lambda_n)$ is the spectral sensitivity of k^{th} photoreceptor class ($k = L, M, S$),

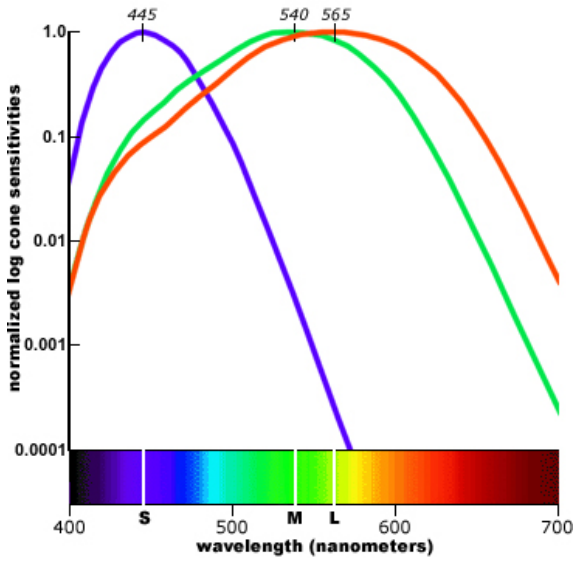

Figure 3.2: Log normalized spectral sensitivity curves; based on the Stockman & Sharpe (2000) 10° quantal cone fundamentals, normalized to equal peak values on a log vertical scale (from http://www.handprint.com/HP/WCL/color1.html).

and λ_n is taken within the visible spectrum.

At the limit when the spectral band is extremely narrow and number of bands N is extremely large, the sum in Formula (3.1) is replaced with an integral over the visible range [WS00]:

$$\rho_k = \int_{380}^{780} C_k(\lambda) I(\lambda) d\lambda. \tag{3.2}$$

As it was stated above, once the energy is absorbed by a photoreceptor, its spectral origin is lost. Thus, two color stimuli with different reflectance values $I_1(\lambda)$ and $I_2(\lambda)$ can, nevertheless, match in color, if the cone responses of L, M and S cones for the two stimuli are equal (Formulas (3.3)). The matching color stimuli are called *metameric stimuli*, or *metamers*, and the underlying concept is referred to as *metamerism* [WS00].

$$\int_\lambda C_L(\lambda) I_1(\lambda) d\lambda = \int_\lambda C_L(\lambda) I_2(\lambda) d\lambda; \tag{3.3a}$$

$$\int_\lambda C_M(\lambda) I_1(\lambda) d\lambda = \int_\lambda C_M(\lambda) I_2(\lambda) d\lambda; \tag{3.3b}$$

$$\int_\lambda C_S(\lambda) I_1(\lambda) d\lambda = \int_\lambda C_S(\lambda) I_2(\lambda) d\lambda. \tag{3.3c}$$

Not only the spectral sensitivities of L, M and S cones are different. Their distribution and proportions across the retina vary as well. When it became possible to take direct images of living human retina (see Fig. 3.3), they provided evidences that cone ratio may vary drastically among individuals [CMNN00, HCN+05, RW99]. Moreover, the ratio and distribution of different types of cones can vary among the two eyes of the same individual and also in different areas of retina. Even more surprising is that, as it has been reported (e.g. in [MPS+98]), individuals with quite extreme cone ratios may still have normal color vision. It is probably due to a proper post processing of signals from the retina and some compensatory mechanisms in the brain.

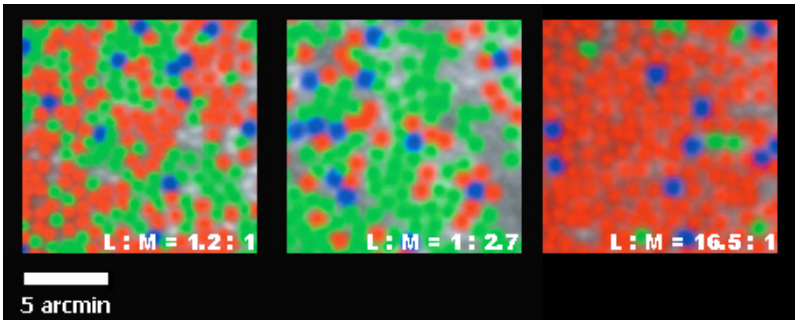

Figure 3.3: The retinal mosaics of three subjects studied. Each figure shows the location of L (red), M (green), and S (blue) cones inpatches of retina at approximately 1-deg retinal eccentricity. The ratio of L to M cones for these subjects is (from left to the right) 1.2:1, 1:2.7 and 16.5:1. The scale bar represents 5 arcmin. All images are shown to the same scale (adopted from Hofer et al., Organization of the Human Trichromatic Cone Mosaic. J. Neurosci. (2005), [HCN+05]).

In spite all the variations in cone distribution, it still seems that there are some "rules" in retinal organization. For example, S cones are generally very rare across the retina and (almost) not present at the central retina (fovea). Furthermore, there is a separate class of bipolar cells making connections only with S cones. It appears to be an invaginating diffuse bipolar cell, connecting with several S cones. All of these add to our poor acuity at short wavelengths [Rob02].

3.1.1 Adaptation

As it was already mentioned in the previous chapter, human visual system is capable of functioning over a huge amount of different illumination conditions. It is adjusted to illuminations of different intensities and with different spectral characteristics, supporting such a crucial feature of human vision as *color constancy* (see

p. 31). The mechanism that provides the adjustment of the visual system to different illumination conditions is called *adaptation*. Three types of adaptation are of particular interest when considering human visual system: *light adaptation*, *dark adaptation* and *chromatic adaptation*.

Light adaptation occurs when the overall level of illumination increases (for example, when turning on a lamp at night in a dark room). Then visual sensitivity decreases to make it possible to see under changed conditions. Within few seconds the visual system is adjusted to the new illumination conditions, and normal visual perception returns. The whole process of light adaptation takes usually less than a minute.

Dark adaptation is an opposite process to light adaptation. It occurs when the overall level of illumination decreases (for example, when entering a dark theater at a sunny afternoon) and results in increasing the visual sensitivity. Unlike the light adaptation, complete dark adaptation takes about 30 minutes. Also, when a person enters a dark room from a light environment (being light adopted), he can not see a thing and is basically blind first. It takes some time until the visual perception starts to return and one is able to see something. Unlike this, when a dark adapted person enters a light room, he is still able to see, although the color perception is distorted first (the contrast is reduced and the colors appear to be washed out).

The third type of visual adaptation, the chromatic adaptation is the most important one while considering color vision properties. It has many aspects and examples (e.g. afterimages and color constancy are supported by the chromatic adaptation). All of them come from a largely independent sensitivity regulation of the mechanism of color vision [Fai98]. Chromatic adaptation does not, probably, lie only in the independent changes of cone spectral sensitivities, but also in the other stages of processing of the visual signal. Chromatic adaptation is a characteristic of visual system that helps to retain the color perception despite the changes in the spectral power distribution of the ambient light (sunlight, daylight, incandesced light, etc.), which often occur in everyday life. Some specific aspects of chromatic adaptation will be described in the "Color constancy" section.

The mechanisms of visual adaptation are not completely understood yet, but some of them include contraction and dilation of the pupil, transitions among rod and cone vision, and the changes in the receptor sensitivities, or *gain control*. The contraction and dilation of the pupil results in reduction or increase of the amount of light, incident upon the retina. However, this does not cover the complete range of differences in illuminations that visual system handles. Additional adaptation mechanisms are required.

The transition between cone (photopic) and rod (scotopic) vision occurs with changes in the light intensity, as it was described in the previous chapter. This transition

is the main mechanism of light and dark adaptations along with the changes in the photoreceptor sensitivities. However, while during light and dark adaptation changes in the photoreceptor sensitivities (gain control) occur simultaneously for all types of cones, during chromatic adaptation the sensitivities change independently for L, M and S cones, according to the conditions.

The adaptation process (especially chromatic adaptation) must be taken into account in the attempts to model human color vision. The adaptation must be considered as a combination of different mechanisms at different levels of visual system. It, probably, involves higher levels of the visual system, like cortex. However, not much of this is known yet.

3.1.2 Color vision deficiencies

As it was stated above, individuals with different cone ratios can still have normal, although differing, color vision. The differences in (normal) color vision are supported also by the lens and macula. They screen short-wavelength energy to different extent, depending on an individual. The properties of the lens and macula can even vary between the left and the right eye of a single individual.

However, not everyone enjoys normal trichromatic vision. About 8% of male, and about 0.4% of female population have one of the forms of *color vision deficiencies* [Fai98]. Those people are sometimes referred to as *color blinds*. This term is misleading, because only a very small percent of people with color deficiencies are real color blinds, unable to discriminate color at all [GS99].

True color blind people are those lacking completely cone photoreceptors, or those, who have only one type of cones. In the first case, individuals are endowed with only scotopic (night) vision, being completely blind at day time. This is called *rod monochromatism*. In the second case individuals are capable to see at high illumination conditions, although their vision is reduced to monochromatic, like it is at night (as was previously explained). This is called *cone monochromatism*. As it was already stated, these kinds of vision deficiencies are very rare.

More common causes of color vision deficiencies are the lack of a particular type of cone photopigment, or alterations in the spectral sensitivities of the photoreceptors. Individuals, who have only two types of cone photopigment, are called *dichromats*. They are still capable of seeing some colors, although color discrimination is altered and all the colors can be matched by only two components. For example, an individual lacking S pigment (a *tritanope*) would not be able to discriminate between the hues in the blue-yellow part of the spectrum (see the “Opponent color theory” section for the explanation), while an individual, lacking either M or L pigment (a

deuteranope and a *protanope*, respectively) can not discriminate between the hues in the red-green part of a spectrum (see Fig. 3.4).

Figure 3.4: Six spectral colors, seen by individuals with different color vision (adopted from www.wikipedia.org).

The alterations in cone spectral sensitivities bring to abnormal trichromatic vision. The alterations can be either the shifts of the spectral sensitivities of different cone types (see Fig. 3.5), or the reduction in their sensitivities. In both cases the ability to discriminate particular hues is reduced. The individuals, suffering these kinds of alterations are called *anomalous trichromats*. Anomalous trichromacy is the most common color vision deficiency (according to [Fai98]).

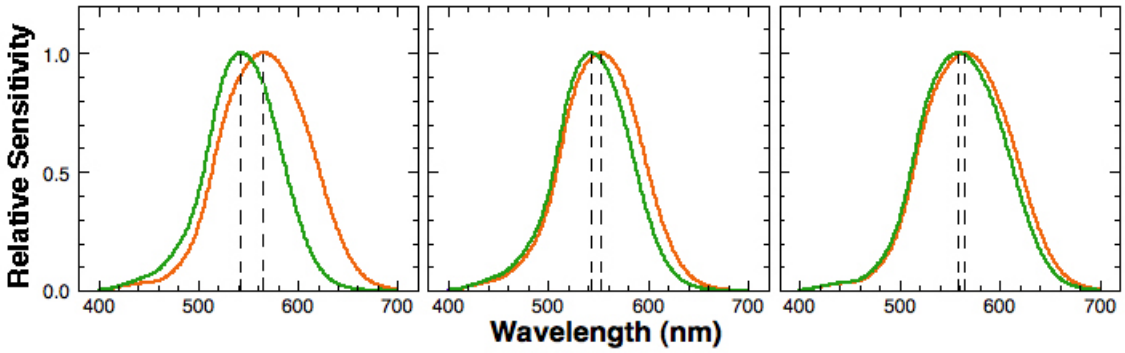

Figure 3.5: Spectral sensitivity curves of M and L cones for normal trichromatic vision (the leftmost image), and for different types of anomalous trichromacy from DeMarco, Pokorny & Smith (1992). Note the shift in the sensitivities.

Different types of color vision deficiencies are common to a considerable percent of human population. Thus, it might be important to take into account those deficiencies in the attempts to model human color vision.

The three cone types are the reason for the trichromatic color vision and for the fact, that each color can be matched by the mixture of three colors, called *primary colors* (see the "Color representations" section). Trichromatic theory was first introduced

and developed already in the middle of the nineteenth century by Thomas Young and Hermann von Helmholtz [You02, Hel52]. It was originally assumed, that the three cone types send their "images of the world" directly to the brain when they are processed for visual perception. However, the trichromatic theory alone could not explain many color vision phenomena, such as afterimages, simultaneous color contrast, as well as the perception of hues by the individuals with color vision deficiencies. The key to deeper understanding of color vision mechanism lies in the *opponent-color theory*, which is the subject of the next section.

3.2 Opponent-color theory

Like the trichromatic theory, the *opponent-color theory*, proposed by Ewal Hering [Her64], occurred as soon as in the end of nineteenth century. However, unlike the well accepted trichromatic theory, the opponent-color theory did not find much support at that time. Only a century later, in the middle of the twentieth century, it became possible to provide some quantitative data, confirming the opponent-color theory.

Hering's opponent-color theory assumes that there are three cone types, however, they have antagonist responses: two chromatic and one achromatic. Based on the evidences, the two chromatic responses were red-green and yellow-blue and the achromatic channel is the luminance channel.

Hering proposed his opponency theory in the attempts to explain some visually observed phenomena, which the trichromatic theory alone failed to explain. First, he noticed that some colors, specifically red and green, and yellow and blue, do not appear together. It is impossible to perceive a reddish green or a yellowish blue[1] while combinations of other colors are possible. This brought him to a conclusion that the two pairs of colors (red-green and yellow-blue) are supported by some fundamental concept of opponency. Still more evidences for that were provided by the opponent nature of the *simultaneous color contrast* phenomena (see p. 31) and the afterimages.

Hering also considered the properties of vision of dichromate observers (those, lacking one of the cone photopigments). He noticed that they lose the ability to discriminate hues in the red-green or yellow-blue part of the spectrum.

[1] More recent experiments have shown that in specially set conditions some observers report the perceived color to be both red and green [CP83]. The discussion of those results is out of the scope of this work and can be found in corresponding literature.

Based on his observations, Hering suggested that there is something more than a simple transition of three separate images formed by the three receptor classes (as it was assumed by the trichromatic theory). He argued that color vision theory must explain the opponent properties, present in all his observations.

A century later Hering's opponent-color theory finally got enough quantitative data support and the explanation for the opponent nature of the color processing was provided at last. The theory of opponency was developed into the so-called *stage theory* of color vision. It represents a combination of the trichromatic theory and Hering's opponent-color theory (Fig. 3.6). It assumes that the first stage of color vision is trichromatic and is based on cone responses. The second stage is the opponency stage which, however, takes place at the post-receptoral level instead of the receptoral level, originally assumed by Hering's opponent-color theory.

According to the stage theory, the *red-green* opponent channel is formed by the responses of L and M cones, while the *yellow-blue* channel results from the difference of S and (M+L) cones (as L and M cones together are responsible for perception of the yellow part of the spectrum). The achromatic channel is formed by L and M cones, although, some models based on the stage theory, like [DVDV93], consider also the influence of S cones on the luminance channel (more details in the next chapter).

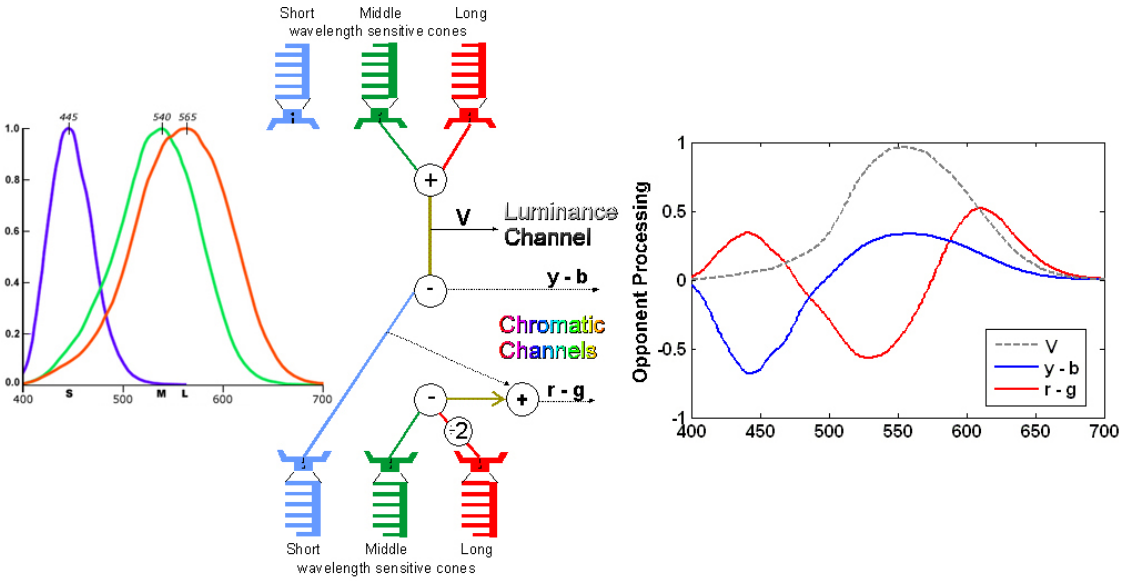

Figure 3.6: Schematic representation of the stage theory, representing encoding of the cone signals into the opponent-channel signals in the human visual system. The cones are represented twice just for convenience.

The vital part in the opponent processing of receptor outputs is probably played by the ganglion cells.

3.2.1 Ganglion cells and opponency

There is a concept of a ganglion cell's *receptive field* - a part of a visual field, sampled by a collection of photoreceptors, whose signals are delivered to the ganglion cell through the intermediate neural layers. The receptive field of a ganglion cell is of a center-surround nature and can be either ON or OFF-centre (Fig. 3.7). In a cell with an ON-centre receptive field (an ON-center cell) light in the centre of the field excites the cell (response increases), while light on the periphery inhibits it (response decreases). It is the opposite case for the OFF-centre cells. This means that an ON-centre cell will respond strongly to a bright spot against a dark background, while an OFF-centre cell will respond to a dark spot on a light background [Rob02].

The centre response of a ganglion cell is usually generated by a single cone, while the surround response is usually driven from signals of several neighboring cones (see Fig. 3.7). In addition to the spatial opponency, there also exists a *spectral opponency*. The midget ganglion cells have a red-green opponency. They receive their central signal from a single L or M cone, while the surround is formed by several cones, which can include both, L and M cones. The blue-yellow cells have receptive fields responsible for the blue-yellow opponency [Fai98, Rob02]. The spectrally opponent ganglion cells are the origins of the color-opponency. The opponent channels continue then through the LGN to the cortex.

Figure 3.7: An example of a red-green ON-center (on the left) and a green-red OFF-center (on the right) spatially and spectrally opponent receptive field.

The opponent-color (stage) theory implies that visual system responds primarily to contrast rather than absolute values [Rob02]. It also represents the "optimization" of the visual information transmission from retina to brain. The opponent signals are more efficient and reduce the noise and correlation between the outputs of different cone types.

3.3 Color constancy

Color constancy is one of the fundamental properties of human color vision. It helps to recognize a color of an object in different viewing conditions. For example, an apple looking red in sunlight will still look red under the incandesced or fluorescent light, although the light signal reaching the eye in different cases may vary significantly. In general, color constancy can be described as a feature of human visual system that helps to maintain the color of an object despite the *variations in the illumination conditions* and despite the *variations in color of the nearby objects*. Without color constancy we would not be able to use the color of an object in an important process of object recognition.

As it was stated in the beginning of the previous chapter, the light signal reaching the eye is a combination of surface reflectance values and energy distribution of the light source (see Equation (2.2) on p. 8). Clearly, the signal will change with the changes in illumination. Human visual system does not support color constancy in the sense, that colors do not look completely the same all the time under varying illumination. However, the visual system does support color constancy in the sense, that it is able to recognize the changes in color as changes in light. To achieve color constancy in the conditions of constantly changing illumination, visual system must have a mechanism to define and remove illumination, i.e. to estimate the reflectance values of an object based on the "available" radiance values. Those estimates are not the exact reflectance values themselves; however they tend to be illumination independent.

Color constancy is supported by several mechanisms of visual system, existing at different levels of the system, staring from the retina. Such a retinal mechanism is chromatic adaptation (p. 24). In the later stages of processing, *memory for color* also plays a part in maintaining color constancy. Actually, adaptation, memory and learning were considered to be the main reasons for color constancy, until the experiments, first held by Edwin Land in 1962 [Lan62]. Land demonstrated that constancy appears not only for familiar objects, whose colors may have been memorized, but for a collage of randomly arranger rectangles of various sizes and colors (see Fig. 3.8). He called such a collage a Mondrian because of the similarities with paintings of a contemporary artist Piet Mondrian. Lands experiment and conclusions he drew are discussed in detail in the next chapter.

Color constancy seems to fail when it is considered as a property of retaining perceived color of an object despite the changes in colors of nearby objects. Moreover, reasons of such failure lie in the same mechanism, supporting color constancy: the mechanism of chromatic adaptation. Examples of such a failure are the *simultaneous color contrast* and *assimilation* phenomena.

Figure 3.8: A sample Mondrian image composed of variously colored and sized overlapping rectangles.

Simultaneous color contrast refers to the changes in the perceived color of an object, depending on its surrounding. Two objects, causing the same response of the photoreceptors will have different color appearance when embedded in different contexts [Rob02]. Color surrounding an object induces its opponent color in the perception of the object (Fig. 3.9(a)). This is caused by the mechanism of chromatic adaptation and color opponency.

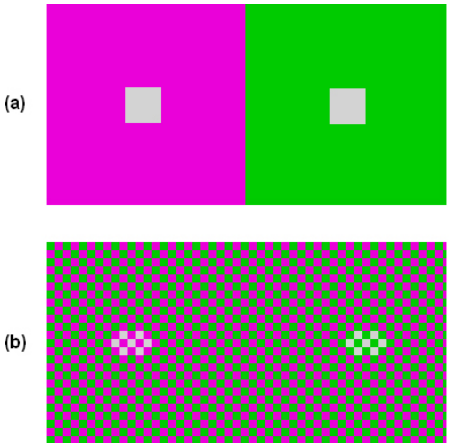

Figure 3.9: (a) The same gray square appears greenish on the pink background and pinkish on the green background due to the simultaneous color contrast. (b) In the different configuration with the same colors the gray rectangle appears pinkish on the left, and greenish on the right, due to the assimilation (the idea adopted from [Rob02]).

Assimilation has an opposite effect, compared with the simultaneous color contrast. The color surrounding the object induces the *same* color as itself in the perception of the object (see Fig. 3.9 (b)). Presence of the simultaneous contrast in some cases

and assimilation in others probably depends on the spatial scale and configuration of the image [Rob02].

Although human visual system reveals the color constancy property only to some extent, it still outperforms most of the existing artificial simulations of the visual system. Models of human color vision must support the color constancy properties to the same extent as they are supported by human observers. The failures of color constancy, such as the simultaneous color contrast must also be considered. In the next chapter one such a model will be discussed.

3.4 Color representations

Even before it had been discovered that there are three classes of cones in the human eye and before it became possible to measure their spectral sensitivities, people realized that most of the perceived colors can be represented by a combination of three colors. This observation was one of the bases to assume, that there are actually three types of cones in the human eye. The colors were called *primary colors* and the combination got the name of *color mixing*.

The main confusion with color mixing occurs because of the difference between *mixing light* and *mixing paints* or dyes. In the first case, color signal reaching the eye consists of all the wavelengths present in all mixed light signals. Each light signal *adds* more wavelengths to the resulting signal. The visual system then is responsible for the light mixing, or *additive color mixing*. For example, if two projectors illuminate a white screen with monochromatic green and red light, the perceived color will be yellow (see Fig. 3.10). This is because the reflected light will contain both, "green" and "red" wavelengths and the photoreceptors will produce the same response as for the monochromatic yellow light. The additive color mixing is used in different self luminous media, such as a monitor or a TV screen.

In the case of mixing dyes, or *subtractive color mixing*, the signal is composed of the light that was not absorbed by the mixed paints. Each additional dye causes a selective *removal* from the light path [Rob02]. The subtractive color mixing is, for example, the base of color printing.

To summarize: the more paints are used in the subtractive mixing, the more wavelengths are *removed* from the light signal reaching the eye; on the contrary, the more light signals are used in the additive mixture, the more wavelengths are *added* to the resulting signal. Thus, additive mixing of the three primaries results in white color, while subtractive mixing of the three primaries may result in black.

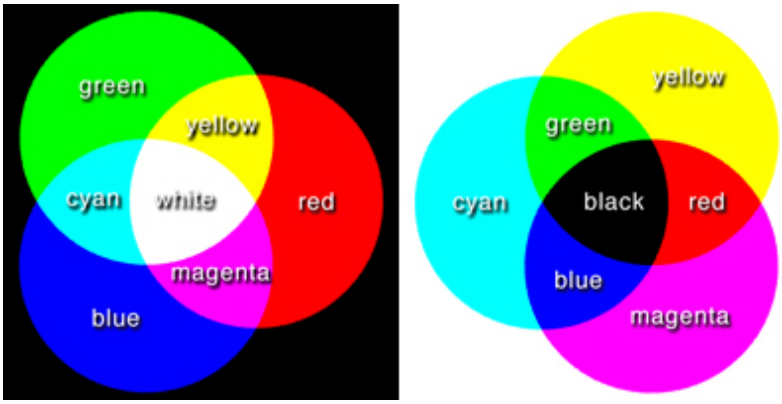

Figure 3.10: Additive (on the left) and subtractive (on the right) color mixing.

For additive color mixing the primaries are usually red, green and blue colors, while for the subtractive mixing cyan, magenta and yellow are used. Those colors are commonly used as primary colors simply because they produce a large gamut of colors (the space of all possible colors that can be produced), although it does not cover all the colors, that can be perceived (see Fig. 3.13 for the gamut of RGB primaries).

3.4.1 Color matching functions

In the early 20^{th} century, without having precise information about the actual sensitivity values of the photoreceptors, CIE had measured the amount of three additive primaries, red ($[R]$, 700 nm), green ($[G]$, 546.1 nm) and blue ($[B]$, 435.8 nm), required to match any *monochromatic* light of a specific wavelength. For each monochromatic light I the corresponding intensities R, G and B of the three primaries $[R]$, $[G]$ and $[B]$ were measured, to match I:

$$I \equiv R[R] + G[G] + B[B]. \tag{3.4}$$

The values R, G and B were called *tristimulus values*.

To obtain the tristimulus values $\overline{r}(\lambda)$, $\overline{g}(\lambda)$ and $\overline{b}(\lambda)$ for a compound spectrum (not a monochromatic light), the *unit* amount of power at each wavelength λ must be matched with an additive mixing of the primaries (see Fig. 3.11). The spectral tristimulus values are called *color-matching functions* [Fai98].

The measurements were held for a small group of observers, first, using 2° visual field and later, 10° field. The 2° color matching functions are referred to as 1931 standard observer. The 10° functions correspond to the 1964 observer.

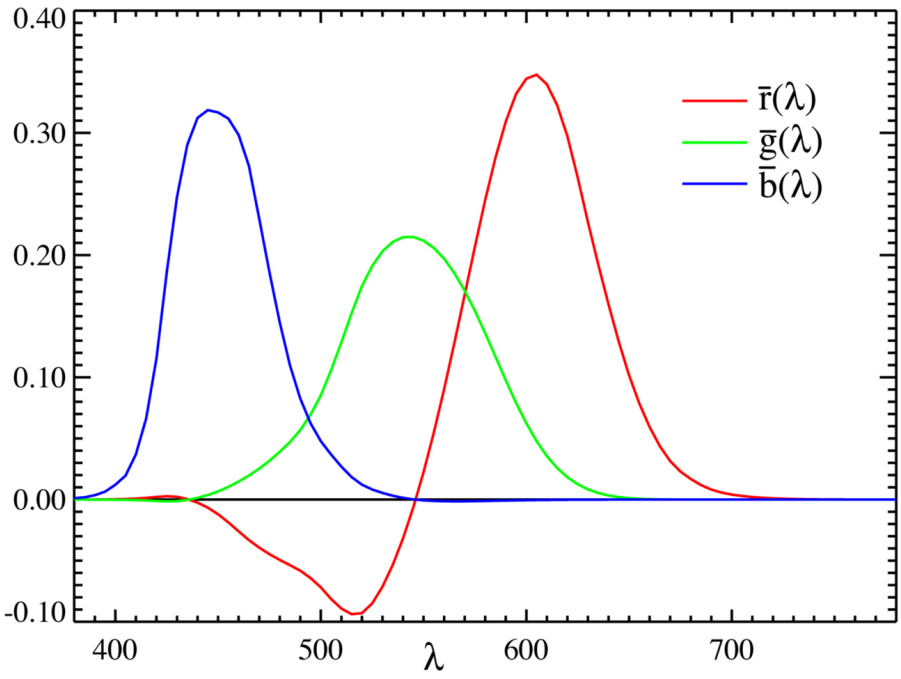

Figure 3.11: CIE color-matching functions $\overline{r}(\lambda)$, $\overline{g}(\lambda)$ and $\overline{b}(\lambda)$ for the $[R]$, $[G]$ and $[B]$ primaries, measured in 1931. The negative values correspond to the fact, that for matching some of the colors, the primaries must be added to the stimuli itself.

To predict the response of the visual system to color stimulus with an arbitrary spectral power distribution $I(\lambda)$ based on the color matching functions, Equations (3.5) can be used:

$$R = \sum_{i=1}^{N} I(\lambda_i)\overline{r}(\lambda_i); \tag{3.5a}$$

$$G = \sum_{i=1}^{N} I(\lambda_i)\overline{g}(\lambda_i); \tag{3.5b}$$

$$B = \sum_{i=1}^{N} I(\lambda_i)\overline{b}(\lambda_i), \tag{3.5c}$$

where the summation is done for each wavelength in the visible spectrum. At the limit, when the spectral band is extremely narrow and number of bands N is extremely large, the sums in Equations (3.5) are replaced with integrals over the

visible spectrum (note Formulas (3.1) and (3.2)):

$$R = \int_{380}^{780} I(\lambda)\overline{r}(\lambda)d\lambda; \tag{3.6a}$$

$$G = \int_{380}^{780} I(\lambda)\overline{g}(\lambda)d\lambda; \tag{3.6b}$$

$$B = \int_{380}^{780} I(\lambda)\overline{b}(\lambda)d\lambda. \tag{3.6c}$$

The tristimulus values depend on the selection of the primaries. However, if two stimuli match in tristimulus values for one set of primaries, they will match for any other set of primaries. The only restriction is that the primaries must be linearly independent, i.e. a primary color can not be matched by additive mixing of two other primaries.

3.4.2 CIE XYZ

After the experiments with RGB color matching functions, CIE suggested using a slightly different set of primaries, mainly to exclude the negative values of the color-matching functions. They denoted the tristimulus values X, Y and Z and the resulting space was named *CIE XYZ color space* (Fig. 3.12). It was the first space based on the human visual properties and it still remains one of the most common spaces in representing the colors an average observer can see.

The tristimulus values in the new space can be transformed to the RGB values with the help of a linear transformation. They also can be transformed to the LMS cone responses (see Appendix B).

The XYZ values can be transformed to the so-called chromaticity coordinates x and y:

$$x = \frac{X}{X+Y+Z},$$
$$y = \frac{Y}{X+Y+Z}.$$

The chromaticity coordinates help to represent the map of the color space, perceived by a standard observer, as it is shown at Figure 3.13 (it is not possible to reflect the correct colors of the map due to the restriction of available gamut). The spectral colors here are situated along the curve called *spectral locus*. The two ends of the

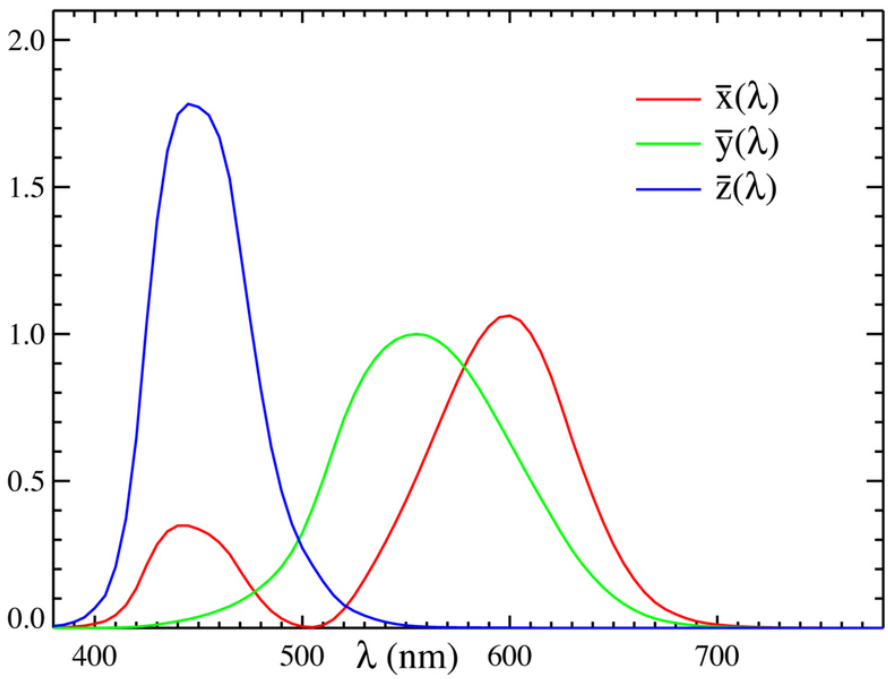

Figure 3.12: CIE XYZ color matching functions $\overline{x}(\lambda)$, $\overline{y}(\lambda)$ and $\overline{z}(\lambda)$ for the X, Y and Z primaries.

locus are connected with a straight line, a *purple boundary*, representing the additive mixing of colors at the ends of the visible spectrum (blue and red). Any color that can be matched by the additive mixture of two other colors in the area, restricted by the locus and the purple boundary, lies on the straight line connecting the mixed colors. The triangle on the picture shows the gamut for the RGB primaries. It can be seen that because of the shape of the chromaticity space, no three primaries can cover all of its area, and thus no three primaries can produce a complete gamut of realizable colors.

There are several color spaces, based on the CIE XYZ. One of them is the CIELAB space with color coordinates L*, a*, and b*. It is also designed to approximate human color vision, referring to the opponent-color theory. CIELAB is more perceptually uniform than the CIE XYZ, meaning that the changes in color closer correspond to the changes in perception. The L* component of the CIELAB model is aimed to represent human perception of lightness, while a* and b* components are opponent color dimensions (red-green and yellow-blue, respectively). CIELAB is used to describe all the colors visible to the observer and even more colors, which can not exist in nature.

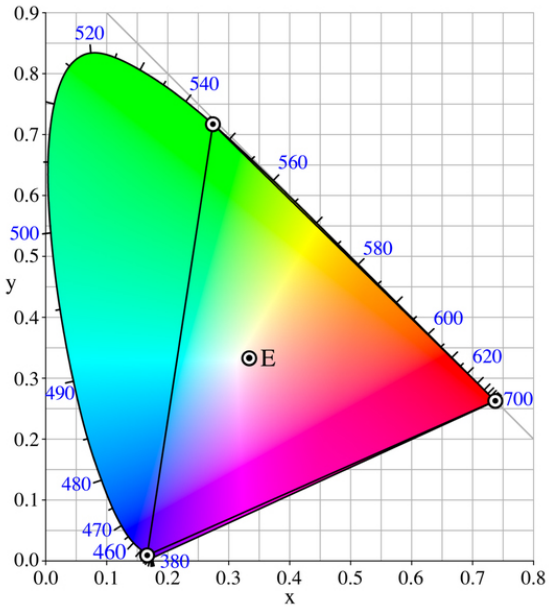

Figure 3.13: Gamut of the CIE RGB primaries and location of primaries on the CIE 1931 xy chromaticity diagram (from http://en.wikipedia.org/wiki/CIE_1931_color_space).

3.4.3 Spectral color representation

Although there are several color spaces, which are based on the properties of the human visual system, it may be worth trying to start with the pure radiance spectrum when modeling color vision. In this way we may be able to avoid the inaccuracy, which inevitably occurs with the use of any particular color space.

The *spectral images* provide us with the required accurate color information, representing the reflectance values for the scene of observation. We can then obtain the radiance values (i.e. the light signal reaching the eye) of a color stimulus for any known illumination, using the Formula (2.2).

The spectral images are stored as sets of several monochromatic images of the same scene (see Fig. 3.14). Each of the monochromatic "slices" (channel) is taken with a different sensor, sensitive to a specific waverange, and represents a set of reflectance values from the range [0, 1].

The use of spectral images provides some additional possibilities when working with color vision models. It becomes easy to obtain the same image under different illuminations, just by using the corresponding spectral power distribution in the Formula (2.2). The spectral image can always be transferred to any other color

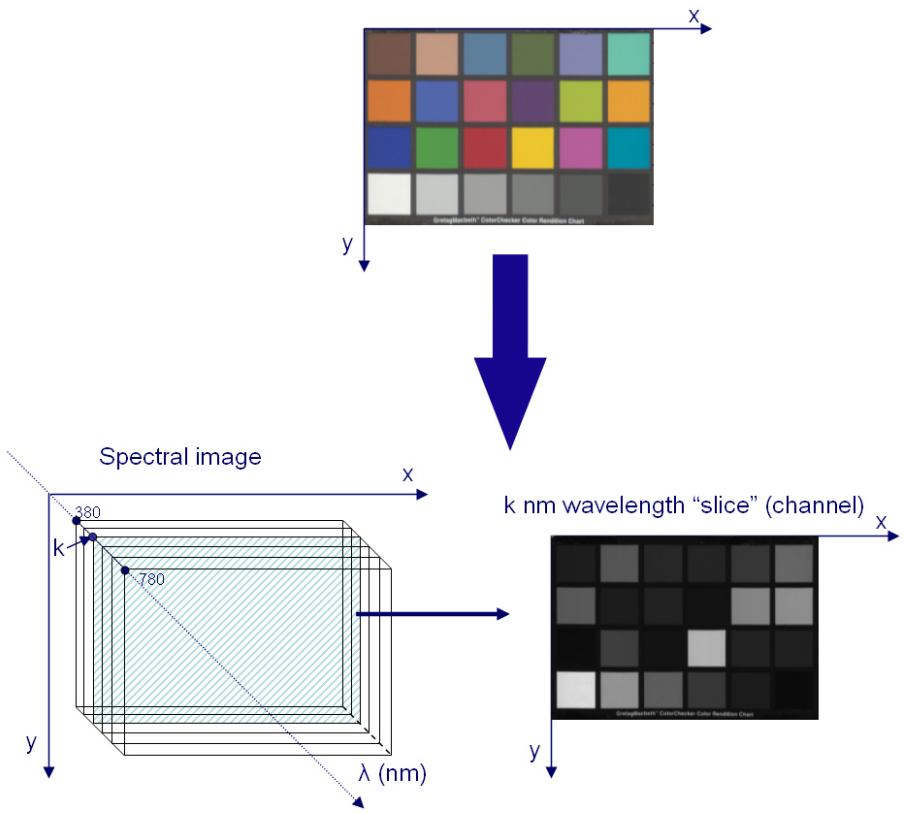

Figure 3.14: Schematic presentation of a spectral image. The RGB representation of the image taken by the spectral camera is at the top. At the bottom is computer representation of the obtained spectra.

representation, as needed (for the comparison or any other purposes). Finally, it may also become useful to know the reflectance values themselves, along with the radiance values.

In the next chapters some of the existing color vision models will be considered. It will be examined, how the use of the spectral images affects the results the models provide.

Chapter 4

Color Vision Models

Nowadays there are multiple color vision models developed by various authors. Each of the models has been designed to serve specific functions of vision, to predict a certain range of vision phenomena, to account for certain perceptual attributes. Even though some of the authors claim the superiority of their models over the other existing ones (e.g. [Gut91]), it is, nevertheless, useful to consider different existing models in order to gain a better understanding of this large field.

Most of the existing models can be classified as being either *neural zone models* or *color appearance models* [CLGP01]. Most of the currently existing neural zone models are based on the stage theory, described in the previous chapter. Physiological and psychophysical evidences prove that simple one stage models are not suitable for modeling human color vision. Based on that assumption, several *multi-stage* models have been developed by various authors. They contain several stages of visual signal processing, which are assumed to take place at different stages of the visual pathways. In this chapter three such models, proposed by Ingling & Tsou [IT77], Guth [Gut91], and De Valois & De Valois [DVDV93] are considered.

Unlike neural zone models, color appearance models usually are not strictly connected to the mechanisms behind some aspects and attributes of color vision. They are based mostly on the psychophysical experiments and observations and are aimed to predict a range of color appearance data. In this chapter one such a model, developed by Land, called Retinex [LM71] is introduced.

4.1 Ingling & Tsou model

In 1977 Carl Ingling and Brian Huong-Peng Tsou introduced their interpretation of the stage theory. They made some assumptions about possible opponent transformation and suggested the orthogonal combination of two opponent channels (*red-green* and *yellow-blue*, further denoted as *r-g* and *y-b*, respectively) and the luminance channel (V_λ), to describe the *visual response* [Ing77, IT77]. The vector model they introduced also supports light adaptation and contains corresponding equations for spectral sensitivities of the opponent channels *near the visual threshold* (before the adaptation) and *above the threshold* (after light adaptation). The underlying concept behind the assumed adaptation mechanism was that adaptation does not cause changes in spectral sensitivities of the photoreceptors. Instead it causes changes in sensitivities of the opponent channels by adjusting weights of corresponding photoreceptors.

Like all the models following the stage theory, the model presented by Ingling and Tsou has the photopigment absorption as its first stage. For this stage they assume Smith and Pokorny cone fundamentals [SP75] (Appendix A). The second stage of the model is opponent and is introduced in both threshold and suprathreshold forms.

The threshold and suprathreshold forms differ in several aspects. The suprathreshold form attempts to take account of the following transformation changes, which where reported at that time by psychophysical and electrophysiological studies to happen with the light adaptation:

- The spectral sensitivity of the *r-g* channel changes with light adaptation, because under certain conditions S cones add to the L cones' signal within the channel.
- For some observers, M cones add to the S cones' signal within the *y-b* channel.
- Rods also add to the S cones' input within the *y-b* channel under specific conditions.

It is assumed, that all the stated transformations for the suprathreshold vision are very much less or completely absent near the threshold.

Let us consider the described changes and stated necessary conditions in more details, starting with the S cones and their contribution to the *r-g* channel. The S and L cones both contribute to the *r-g* channel in the similar way: they suppress the signal from the M cones and thus result in increasing perception of red. However, unlike the L cones, the S cones affect the *r-g* channel only when there is an M signal

to inhibit. Otherwise, only the L cones are responsible for the perception of red. Thus, the contribution of S cones occurs only with the light adaptation (especially with white light adaptation), when the M cones become active. The distinctions between the sensitivity curves for the r-g channel before and after adaptation are illustrated in Figure 4.1. It is apparent, that the r-g sensitivity curves differ in their shapes, which can not be represented merely by a scaling factor (unlike the y-b channel curves).

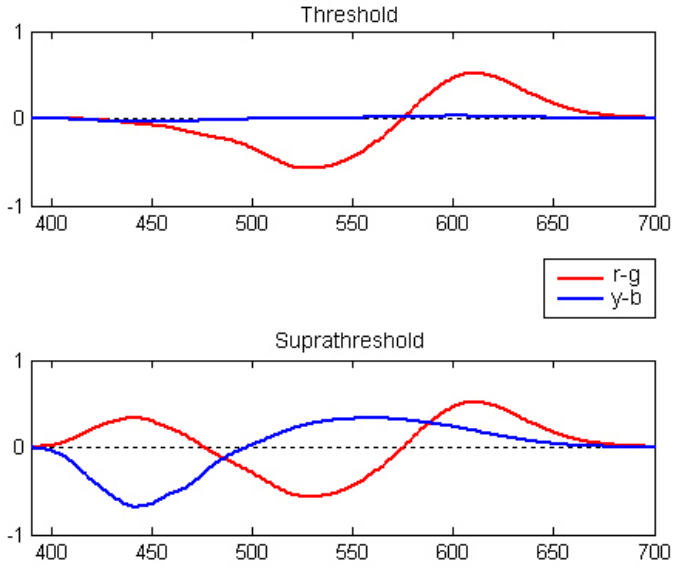

Figure 4.1: Spectral sensitivity curves for the opponent r-g and y-b channels: near threshold (top) and moderate intensity levels (bottom).

When considering the y-b channel, there are two possible changes around the threshold. First, for about 20% of the population, M cones add to the signal of the S cones within the y-b channel by suppressing the $y = (L + M)$ signal [Ric67]. However, this happens only with light adaptation, in the case of a present y signal (alike the behavior of S and M cones in the previously described situation with the r-g channel).

Second possible factor is the rod signal mixing with the S cone signal within the y-b channel. This causes the inhibiting of y channel and happens also when there is a y signal. However, unlike the previous case with the M cones' signal, this happens only within a short range of mesopic vision, when both rods and cones are active.

Figure 4.2 summarizes the considered differences.

The equations (4.1) and (4.2) represent the corresponding transformations of the

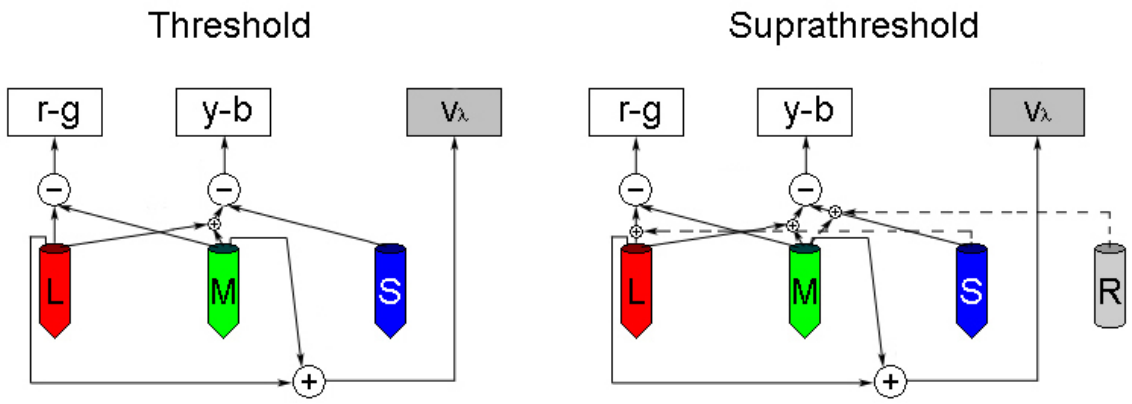

Figure 4.2: Opponent color diagram. The diagram on the left shows the connections for the threshold transformation. The diagram on the right is the same diagram for the suprathreshold transformations. Red, green and blue elements of the diagram represent L, M and S cones, respectively. The gray cylinder represents rods. (Adopted from [IT77]).

LMS cone signals to the opponent *y-b*, *r-g* signals and achromatic V_λ signal for the threshold and suprathreshold conditions, respectively [IT77].

Threshold form:

$$r - g = 1.2L - 1.6M; \tag{4.1a}$$
$$y - b = K_1(0.24L + 0.18M) - K_2(0.7S) - 0.075M; \tag{4.1b}$$
$$V_\lambda = 0.6L + 0.4M; \tag{4.1c}$$
$$K_1 = 0.2, \quad K_2 = 0.06. \tag{4.1d}$$

Suprathreshold form:

$$r - g = 1.2L - 1.6M + 0.4S; \tag{4.2a}$$
$$y - b = K_1(0.24L + 0.18M) - K_2(0.7S) - 0.075M; \tag{4.2b}$$
$$V_\lambda = 0.6L + 0.4M; \tag{4.2c}$$
$$K_1 = K_2 = 1. \tag{4.2d}$$

If a *receptive field operator* θ is introduced [Ing77], the equations (4.1) and (4.2) are reduced to a single set (4.3):

$$r - g = -(-1.2L + 1.6M\theta 0.4S); \tag{4.3a}$$
$$y - b = K_1(0.24L + 0.18M) - K_2(0.7S) - 0.075M. \tag{4.3b}$$

The operator θ is defined as follows:

$$\forall a, b \quad (a\theta b) = \begin{cases} (a-b) & \text{if } a > b; \\ a & \text{if } a \leq b. \end{cases} \tag{4.4}$$

and values K_1 and K_2 are dependent of the threshold form.

As it was mentioned above, Ingling and Tsou [IT77] suggested a vector space to represent the model's *visual response* to a light signal. The axes of this space represent the opponent and the luminance channels, as shown in Figure 4.3. A vector, defined in such space by its *r-g*, *y-b* and V coordinates, represents the *visual response*, denoted as S, to a light signal Q:

$$S^2 = Q^2[(r-g)^2 + (y-b)^2 + V_\lambda^2]. \tag{4.5}$$

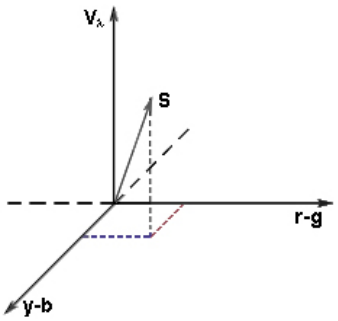

Figure 4.3: Illustration of the vector space.

The vector model introduced by Ingling and Tsou is rather simple. However it proves to be useful in estimating the outcomes of several color vision experiments (e.g. discrimination experiments). The results of such an experiment will be introduced in the next chapter, along with some demonstration of the transformation from RGB to *r-g*, *y-b*, V space.

4.2 Multistage color vision models

The Ingling & Tsou model contained a single opponency stage. This was mainly due to the lack of information about the signal processing within the visual pathways at that time. The following growth of the theory about the real processes behind the opponency stage caused the new direction in development of color vision models. The opponency stage, assumed by the stage theory, was divided to several parts, one happening in the retina, and the others, further in the visual pathways. Two of such models are introduced in this section.

4.2.1 Multi-Stage Color model by De Valois & De Valois

Model developed by Russell and Karen De Valois in 1993 [DVDV93] was named a *Multi-Stage Color Model*. It consists of three stages and represents an enhancement of the classical stage theory by containing two opponent stages, instead of just one.

The first stage of the model represents the absorption of the light signal by cone photoreceptors. Here, the spectral sensitivities of cones are also obtained from Smith and Pokorny data [SP75], which takes into account the preretinal absorption, happening in the lens and macula. Main assumption in the first stage is about the distribution of different types of cones in the retina. Firstly, De Valois and De Valois assume that S cones are arranged regularly, while L and M cones are arranged randomly; secondly, they propose the proportions of L:M:S cones in the retina to be 10:5:1. All the calculations of the following stages are based on those assumptions.

The second stage of the model is based on anatomical evidences and assumptions. It models the formation of opponent signals from cone responses, happening in the retina. Although it is not clear yet, at which (plexiform) layers of the retina certain interactions take place, there are some assumptions about the type of such interactions. The basic underlying principle behind the second stage is that a (midget) bipolar cell gets direct input from a single cone in the center and indirect input from a horizontal cell, connecting several surrounding cones. The indirect input from horizontal cell is further subtracted by the bipolar cell from the direct cone input. Two versions of the second stage are represented, based on the possible suggestions about the behavior of horizontal cells. The *indiscriminate* version suggests random connectivity of horizontal cells, without differentiating between the cone types. The *discriminate* version, on the contrary, suggests that if the corresponding bipolar cell has a direct input from L cone, then the indirect input from the horizontal cell will be composed of the responses of M cones only (and vice versa). The results after the third stage of the model are much alike for both versions of the second stage. However recent anatomical evidences support the indiscriminate version of the model with largely random connectivity [DVDV93]. Thus further the indiscriminate version will be considered.

The second stage of the model defines six cone-opponent outputs: L_o, M_o, S_o, as it is shown in the Equation (4.6) below, as well as their negative versions $-L_o$, $-M_o$ and $-S_o$:

$$\begin{bmatrix} L_o \\ M_o \\ S_o \end{bmatrix} = \begin{bmatrix} w_m + w_s & -w_m & -w_s \\ -w_l & w_l + w_s & -w_s \\ -w_l & -w_m & w_l + w_m \end{bmatrix} \begin{bmatrix} L \\ M \\ S \end{bmatrix}, \tag{4.6}$$

where w_l, w_m and w_s are the weightings of L, M and S, respectively [JHP+07]. This is a generalization of the original model, where the weightings were fixed to be equal

to 10, 5 and 1, respectively, and represented the assumed cone ratio [DVDV93].

The third stage of the model is assumed to be the perceptual opponency, happening during the cortical processing. From the outputs of the second stage two chromatic signals RG and BY, and one achromatic signal A are formed, as represented in the Equation (4.7) [JHP+07]:

$$\begin{bmatrix} RG \\ YB \\ A \end{bmatrix} = \begin{bmatrix} +1 & -1 & +1 \\ -1 & +1 & +1 \\ +1 & +1 & +1 \end{bmatrix} \begin{bmatrix} w_l & 0 & 0 \\ 0 & w_m & 0 \\ 0 & 0 & 2w_s \end{bmatrix} \begin{bmatrix} L_o \\ M_o \\ S_o \end{bmatrix}. \tag{4.7}$$

Thus, the color and luminance information is separated. The schematic representation of the third stage of the model is represented in Figure 4.4 below.

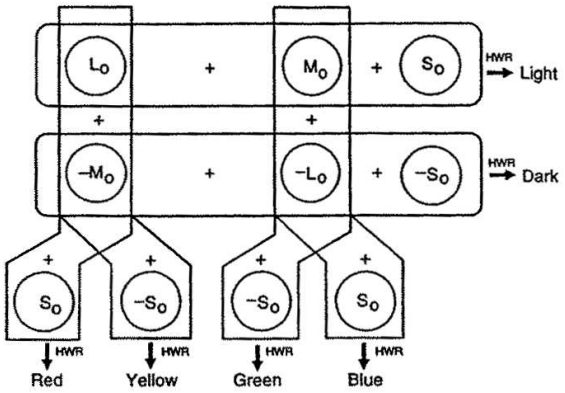

Figure 4.4: Complete diagram of the processing stage 3 (from [DVDV93]).

The Multi-Stage Color Model supports much of the anatomical and physiological evidences concerning the opponency, happening both at the retinal and cortical level. However, it is tied strictly to the distribution of cones in the retina. As it was discussed in the previous chapter (see p. 24), cone distribution varies significantly among the individuals with normal color vision [CMNN00, HCN+05, MPS+98, RW99]. Thus, this kind of models, related strongly to the distribution of cones, must, probably, be reconsidered in order to support these recently emerged evidences.

The Multi-Stage model also does not support such an important mechanism of visual system as adaptation. A model, described in the next section, overcomes this shortcoming by including an adaptation mechanism in its first stage. However, it is inferior to the Multi-Stage Color Model in the respect of having less physiological and anatomical bases.

4.2.2 Guth's Model for Color Vision and Light Adaptation

In 1991 S. Lee Guth consolidated all his previous work in the field of color vision, as well as the work carried by other scientists in the field, by proposing a *Model for Color Vision and Light Adaptation* [Gut91], he called *CA90*. The CA90 model incorporates several mechanisms of human visual system, starting with the photoreceptor *absorption* and *adaptation*, and going through two *successive opponent stages*: one happening in the retina, and the other later in the visual pathway [Gut91]. The model is capable of predicting a wide range of data on several visual phenomena, such as chromatic and light adaptation and chromatic discrimination [Fai98].

During the following years, Guth suggested some improvements and modifications to his original CA90 model. The latest version of the model was published in 1995 [Gut95] and is referred to as the *ATD95* model. Further, when talking about the ATD model in general, we will assume a model consisting of stages, described by Guth. The exact model will be specified when talking about the parameters of the model. We will further concentrate mainly on the last edition of the model (ATD95), making comparisons with the CA90 version. More detailed comparative analysis can be found in [CLGP01].

Figure 4.5 shows a schematic representation of Guth's ATD model. The letters A, T and D stand for the *achromatic*, *tritanopic* and *deuteranopic* mechanisms, supported by the two opponent stages of the model. At the first stage of ATD model the input tristimulus values are transferred to LMS cone response values. The input values are the modification of CIE XYZ (1931) values by Judd [Jud51] and Voss [Vos78]. The LMS responses are obtained according to Smith and Pokorny cone fundamentals [SP75]. The LMS values are further normalized and multiplied by weighting factors. In the CA90 the weights were 0.66, 1 and 0.55 for L, M and S responses, respectively. In the ATD95 only the weight for S response has been modified from 0.55 to 0.43, while other weighting factors remained unchanged. Those weights are chosen experimentally to provide the model with certain desirable features. They are not intended to reflect cone distribution differences in the human retina.

After the weighting, cone responses undergo a nonlinear transformation of exponentiation, after which photoreceptor noise is added to the modified LMS values. In the CA90 model noise was identical for each channel and was equal to 0.00004. In the ATD95 model noise signals are: 0.024 for the L; 0.036 for the M and 0.31 for the S channel.

Finally, the adaptation, or *gain-control* (denoted as GC in Figure 4.5) is introduced

by a nonlinear transformation (4.8) in CA90 and (4.9) in ATD95.

$$N_g^{(1)} = N\left[1 - 0.99\frac{\sigma}{\sigma + N}\right], \tag{4.8}$$

$$N_g^{(2)} = N\left[\frac{\sigma}{\sigma + N}\right], \tag{4.9}$$

where N is the receptor's (L, M or S) response, modified as described above and σ is a positive number. In the CA90 $\sigma = 0.05$ and changes with adaptation, while in ATD95 $\sigma = 300$ permanently.

The second and the third stages of the model represent two opponent mechanisms. The attenuated by the gain-control L, M and S signals feed into the *first opponent stage*, yielding an *achromatic* (A_1) and two *opponent* (T_1 and D_1) signals. The *initial* A_{1i}, T_{1i} and D_{1i} responses are calculated using transformations (4.10):

$$\begin{bmatrix} A_{1i} \\ T_{1i} \\ D_{1i} \end{bmatrix} = M_1 \times \begin{bmatrix} L_g \\ M_g \\ S_g \end{bmatrix}, \tag{4.10}$$

where the CA90 and ATD95 transformation matrixes $M_1^{(1)}$ and $M_1^{(2)}$ are represented in (4.11):

$$M_1^{(1)} = \begin{pmatrix} 0.4200 & 0.3108 & 0 \\ 0.8845 & -0.7258 & 0 \\ -0.0770 & 0.01301 & 0.091 \end{pmatrix}, \tag{4.11a}$$

$$M_1^{(2)} = \begin{pmatrix} 3.57 & 2.64 & 0 \\ 7.18 & -6.21 & 0 \\ -0.70 & 0.085 & 1 \end{pmatrix}. \tag{4.11b}$$

The initial A_{1i}, T_{1i} and D_{1i} responses, in turn, feed into the *second opponent stage*, yielding the A_2, T_2 and D_2 signals, similar to Hering's opponent signals: *luminance*, *red-green* and *yellow-blue*, respectively:

$$\begin{bmatrix} A_{2i} \\ T_{2i} \\ D_{2i} \end{bmatrix} = M_2 \times \begin{bmatrix} A_{1i} \\ T_{1i} \\ D_{1i} \end{bmatrix}, \tag{4.12}$$

where the CA90 and ATD95 transformation matrixes $M_2^{(1)}$ and $M_2^{(2)}$ are represented

in (4.13):

$$M_2^{(1)} = \begin{pmatrix} 0.1 & 0 & 0 \\ 0 & 0.388 & 1 \\ 0 & 0 & 1 \end{pmatrix}, \tag{4.13a}$$

$$M_2^{(2)} = \begin{pmatrix} 0.09 & 0 & 0 \\ 0 & 0.43 & 0.76 \\ 0 & 0 & 1 \end{pmatrix}. \tag{4.13b}$$

The final step of both, first and second opponent stages represents a *nonlinear compression* (4.14) to get final A, T and D responses:

$$F_f = \frac{F}{\sigma_c + |F|}, \tag{4.14}$$

where F is the uncompressed initial signal of an opponent stage (A_{1i}, T_{1i}, D_{1i} and A_{2i}, T_{2i}, D_{2i}).

The first opponent stage of Guth's model mediates apparent *brightness* and is also responsible for "small step" color *discrimination* and detection (discrimination from noise). The brightness of a stimulus is the norm of the vector characterizing the stimulus in the $A_1T_1D_1$ space:

$$Br = \sqrt{{A_1}^2 + {T_1}^2 + {D_1}^2}.$$

For *small difference* discrimination of two light signals with calculated A_1, T_1 and D_1 values, the Euclidean distance between the two vectors is calculated:

$$\Delta E_s = \sqrt{\Delta{A_1}^2 + \Delta{T_1}^2 + \Delta{D_1}^2}.$$

If ΔE_s becomes greater than the discrimination threshold, there is a just noticeable difference between the two tested color signals. According to [Gut95], the most appropriate threshold value for predicting a wide variety of discrimination and detection results is 0.005.

The second opponent stage ($A_2T_2D_2$) mediates *hue* and *saturation* and is responsible for *large* color differences:

$$H = \frac{T_2}{D_2}; \tag{4.15}$$

$$S = \frac{\sqrt{{T_2}^2 + {D_2}^2}}{A}; \tag{4.16}$$

$$\Delta E_L = \sqrt{\Delta{A_2}^2 + \Delta{T_2}^2 + \Delta{D_2}^2}. \tag{4.17}$$

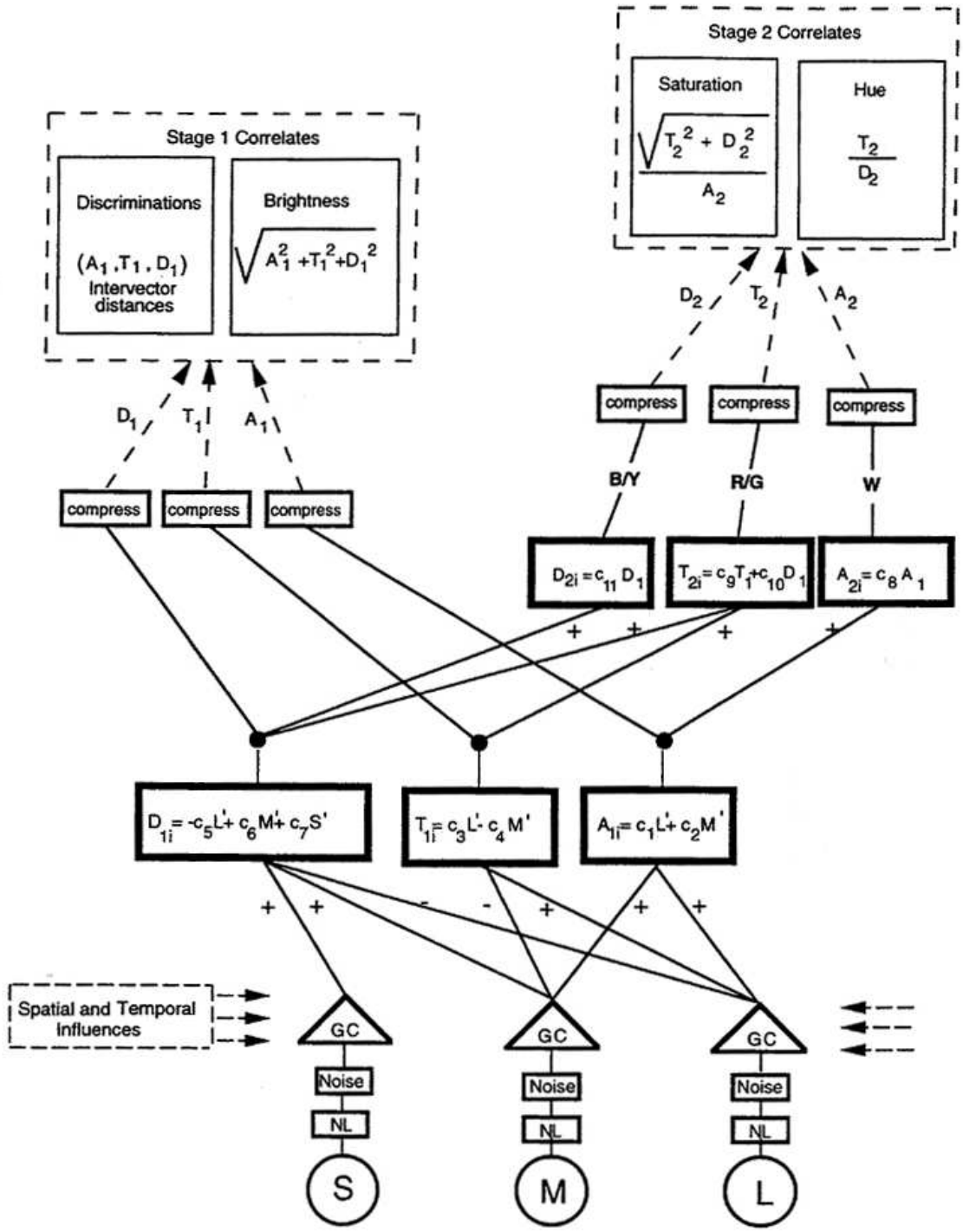

Figure 4.5: Schematic diagram of Guth's model ([Gut95]).

Although the ATD model provides all the necessary color information due to its red-green, yellow-blue and achromatic channels, it does not specify an apparent way to predict color appearance. However, it is able to predict various visual phenomena and is appropriate for different discrimination and comparison experiments.

4.3 Retinex color appearance model

All the models described above are designed to deal with unrelated colors, or colors perceived in isolation. Guth has stated [Gut98] that his model is appropriate for related color stimuli as well, or stimuli within a visual field containing several color areas. However, in practice some, yet unclear modifications must be introduced to the model in order to deal with the related color stimuli [Fai98].

Unlike the models described above, the model introduced in this section was designed to deal with related color stimuli, or color stimuli within a complex visual field. It is called *Retinex* and was the first attempt to model one of the fundamental features of human color vision, color constancy (see p. 31).

The Retinex theory for color computation was first introduced by Land in 1964 and was further published in the Journal of the Optical Society of America [LM71]. For his color constancy experiments Land used a laboratory display he called a Mondrian (see Fig. 3.8 on p. 32), consisting of about 100 colored paper rectangles [Lan83]:

> "A paper of a given color would appear many times in different parts of the display, each time having a different size and shape and each time being surrounded by a different set of other colored papers."

The Mondrian was illuminated with three independently adjustable light projectors, providing light of short (around 450 nm), middle (around 550 nm) and long (around 650 nm) wavelengths. A light detector was measuring the light signal reflected from any particular area of the Mondrian (Fig. 4.6).

In the beginning of the experiment the intensities of the three projectors were set in such a way, that the observers reported the Mondrian to look deeply colored. Then light detector measured the light signal coming from a particular, say white, area of the display. Three radiance values I_L, I_M and I_S were obtained using one projector (and hence, one waveband) at a time. Next, the detector was turned to another, say green, area and the light projectors were adjusted so, that the three radiance values were again I_L, I_M and I_S, like for the white rectangle. However,

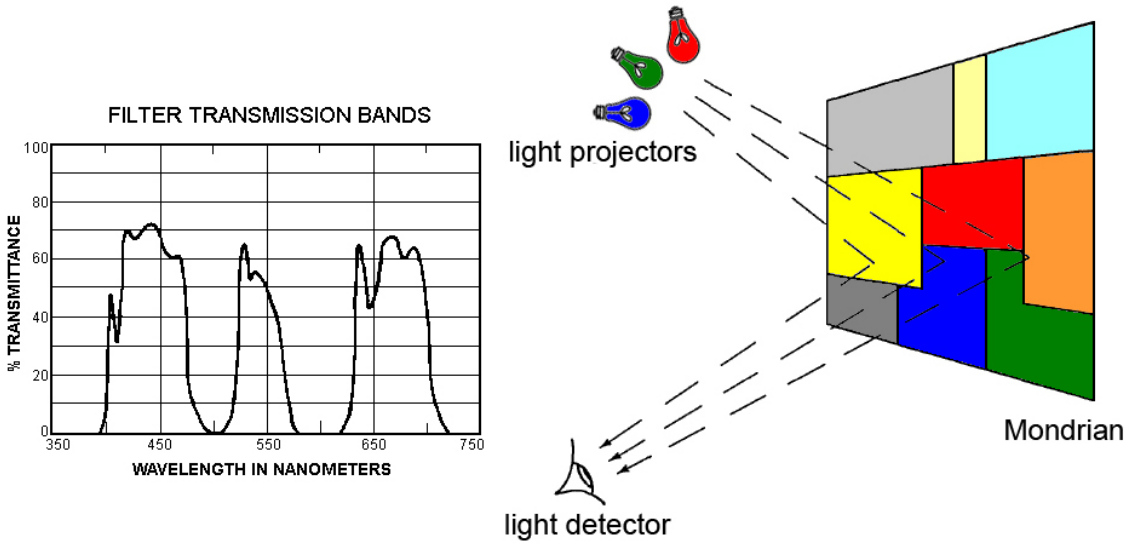

Figure 4.6: Illustration of Land's experiments with Mondrian-like displays. Spectral characteristics of the light projectors are represented on the left (adopted from [LM71] and [BW86]).

the observers reported that color sensation remained essentially unchanged and the rectangle still looked green. The same experiment was performed for all the color rectangles of the Mondrian. In all the cases the areas continued to generate the same color sensations with just slight differences, despite the fact, that the radiance values were set to be the same (I_L, I_M and I_S) for all rectangles.

To summarize, the experiments showed that the same radiance values may produce different color sensations. Based on this, Land concluded that the color sensation of an arbitrary area of the visual field can not be obtained exclusively from the product of the illumination and the reflectance of that isolated area (although it seems to be the only information reaching the eye). In reality, the visual system gets information from the entire visible scene. This information is used to eliminate the effect of the unknown and non-uniform illumination and helps to provide color constancy [PJH+07].

Land suggested that color sensation involves processing of the spatial information from the visible scene with several independent systems, each of which he called a *Retinex*. Originally the name "*Retinex*" came from the combination of the words "*retina*" and "*cortex*". This illustrates Land's suggestion about three retinal-cortical systems [LM71]:

> "Each system forms a separate image of the world; the images are not

> mixed but are rather compared. Each system must discover independently, in spite the variation and unknown properties of the illumination, the reflectance for the band of wavelengths to which that system responds."

The systems were assumed to be sensitive to the short, middle and long wavelengths.

There are several published versions and modifications of the original Retinex algorithm described, for example, in [Lan86], [JRW97], [KES+03], [XF06]. However, the consideration of these modifications is out of the scope of this work. Within the classical Retinex theory, the variations between the algorithms are mainly aimed to improve computational efficiency, rather than the model itself, such as, for example, the pyramid approach in the [FM38].

In the originally proposed Retinex algorithm the input data represented an array of short-, middle- and long-wavelength sensitive photoreceptor responses for each pixel of an image [BW86]. Algorithm calculated the so-called *lightness values*, defined as biological correlates of the reflectance values [LM71] for each pixel of the image and each photoreceptor class by a scheme described below.

The main concept of the algorithm is the comparison of pixels in the image. This is done by accumulating lightness values along the paths of pixels. Each path starts with the pixel, whose lightness value is considered to be the maximum along the path. The values obtained from different paths are combined to estimate the output lightness value.

Each of the iterations of the Retinex algorithm represents a combination of four steps: *ratio*, *product*, *reset* and *average*[1]. *Ratio* is used to compare nearby pixels. For two pixels the ratio of the radiance of the second pixel and the estimated lightness of the first pixel is calculated to estimate the lightness value of the second pixel. *Product* of ratios is used for long-distance interaction and is calculated for each path (Fig. 4.7). Calculation starts with the current radiance value at one pixel and multiplies the value by the ratio of comparison pixel (next pixel in the path) and starting pixel; the new product is the current lightness value of the comparison pixel.

Reset step is used to find the pixel with the highest lightness along the path. In the beginning, the first pixel of the path is assumed to have the highest lightness value. Then one moves through the path and calculates the sequential product. Whenever one meets a pixel, for which the sequential product becomes greater than 1, it means that the pixel's lightness is higher than first pixel's lightness. Thus

[1]The original algorithm also included a so-called threshold step, which was omitted in the further modifications of the algorithm, as no psychophysical support was found for it [McC99].

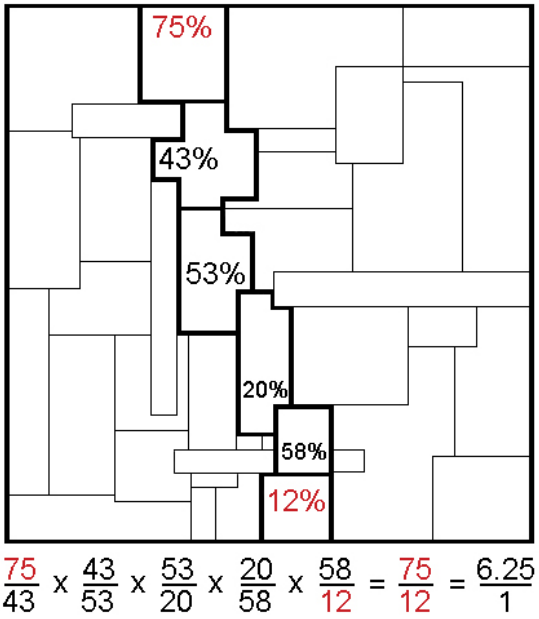

Figure 4.7: Reflectance along one path between the top and bottom of a black-and-white Mondrian (the top and bottom reflectance values are marked with red, for clearness). The numbers at the bottom indicate the ratios of reflectances at adjacent edges along the path (adopted from [LM71]).

this new pixel is assumed to have the highest lightness and the path starts afresh from that pixel. The reset step represents independent normalization of L, M and S responses to the corresponding maximum values within the visual field. It has been experimentally proven that human visual system performs similar independent normalization [McC99].

Finally, at the *average* step the average of all calculated sequential products for all considered paths ending in a single pixel is taken to obtain the lightness value for that pixel.

The original goal of the Retinex model was to predict the color sensation from the visual field without a prior information about the light source or reflectance values. It was aimed to show that color constancy can be predicted by spatial comparisons without modeling photoreceptor adaptation [LM71, McC04].

In general, color constancy models may be divided into two groups. First group consists of the algorithms aimed to achieve *absolute color constancy*. The ultimate and yet unreachable goal for this kind of models is to estimate reflectance values from the available radiance values with unknown and possibly non-uniform illumination.

The second group, to which the Retinex model belongs, consists of the models aimed to predict *human color constancy*. The models should support such failures of color constancy as simultaneous contrast and assimilation (see p. 31). However, there is no single model that predicts both assimilation and contrast yet [McC04], probably, because it is not clear yet in which cases each of the effects appear. In the next chapter two color constancy experiments performed with the Retinex model will be described, one of which demonstrates that the model supports simultaneous color contrast.

It has been admitted [McC99] that Retinex can not serve as a model for absolute color constancy, i.e. it can not separate illumination from reflectance. However, in the next chapter we will see that within some conditions the output of the Retinex has considerable similarities with the reflectance spectra.

Chapter 5

Experiments and Evaluation

The next step in studying color vision models is the model evaluation. It is necessary to estimate how well the considered models describe human color vision. However, as soon as each model is aimed to serve for a certain set of functions only, there can not exist a single test, which will help to evaluate all the models and compare them in terms of their performance. Each group of models requires a separate set of specially designed tests.

Although the approaches to modeling and evaluation differ among the considered models, there is a single aspect that unites them all. The main approach of this work is to use the *spectral images* (see p. 38) rather than other color representations during modeling, as well as during the evaluation. This provides accurate color information, independent on the illumination conditions and observer. Thus, it seems to be a proper "raw" data for color vision models, and helps to avoid any discrepancies already at the early stages of modeling.

The first section of this chapter describes the tests designed and performed for the Ingling and Tsou vector model. The second section is dedicated to the Retinex model, its performance and possible ways of applying the model to spectral images.

Since this chapter represents the main approaches and methods proposed within the limits of this work, each section is followed by short conclusions, summarizing the main achievements and possibilities for future work.

5.1 Ingling & Tsou model

In this section we return to the vector model introduced by Ingling & Tsou and described in the previous chapter of this work. Here some approaches for its evalu-

ation are represented. They can also be used for the evaluation of similar models, as those described in the previous chapter (see p. 44).

5.1.1 Wavelength discrimination

The wavelength discrimination experiment consists in determining the smallest noticeable variation $\Delta\lambda$ in the wavelength λ. A typical discrimination experiment is called a method of "*least noticeable differences*" [BW58]. Given a bipartite field illuminated with a monochromatic light of wavelength λ, the observer is asked to adjust one of the halves of the field so, that it becomes just *barely distinguishable* from the other half of the field. Typically, the attempt is made to keep the light intensity constant while changing the wavelength λ. The observer first sets the least noticeable difference by shifting λ towards longer wavelengths $(+\Delta\lambda)$, and then does the similar settings towards the shorter wavelengths $(-\Delta\lambda)$. Those measured values can be further combined to obtain the average difference $\overline{\Delta\lambda} = [(+\Delta\lambda) + (-\Delta\lambda)]/2$ for each tested wavelength λ. Either $(+/-)\Delta\lambda$, or $\overline{\Delta\lambda}$ values are then plotted against the corresponding wavelengths, and the observation points are joined by straight lines to represent the wavelength discrimination curves, as shown in Figure 5.1 below.

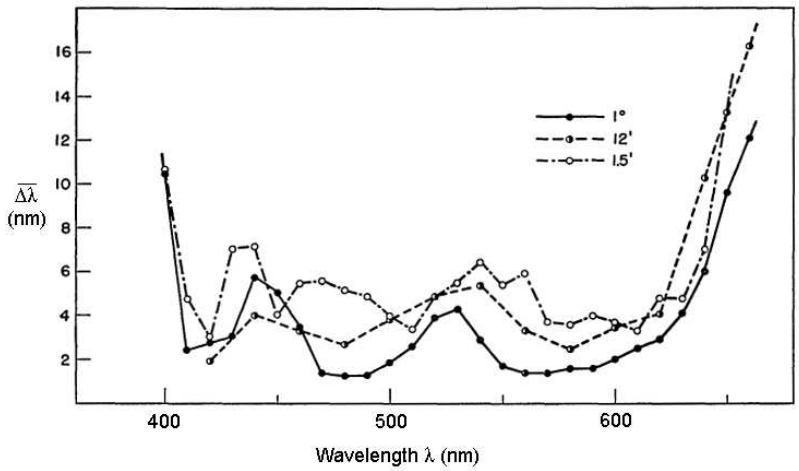

Figure 5.1: Wavelength discrimination curves. Observations were made by a single observer for different field size and retinal illumination ([BW58]).

Bedford and Wyszecki have shown [BW58] that wavelength discrimination curves vary among observers, as well as with the changes in the light intensity and visual field size. They also represented data concerning color vision of point sources (a 1.5' visual field), which is the most appropriate for our experiments.

The wavelength discrimination experiment was performed for the MATLAB^{TM} implementation of Ingling & Tsou vector model. The light adapted (suprathreshold) conditions were considered. Spectral sensitivities of photoreceptors were obtained from Stockman and Sharpe (2000) 2-deg cone fundamentals [SSF99, SS00] (Appendix A). The experiment was conducted for the wavelength range from 380 nm to 650 nm with the step of 10 nm, to connect with the real human data from Bedford and Wyszecki. A monochromatic light signal of wavelength λ was modeled as a set of reflectance values for a single pixel, in the specified waverange (with a step of 1 nm). This can be considered to be the analogue of the point light source, considered by Bedford and Wyszecki. The reflectance value for wavelength λ was set equal to 1, while the values at remaining wavelengths were set equal to 0. The responses of the model to the monochromatic light of different wavelengths were calculated using formulas (4.2) and (4.5) on pages 43-44.

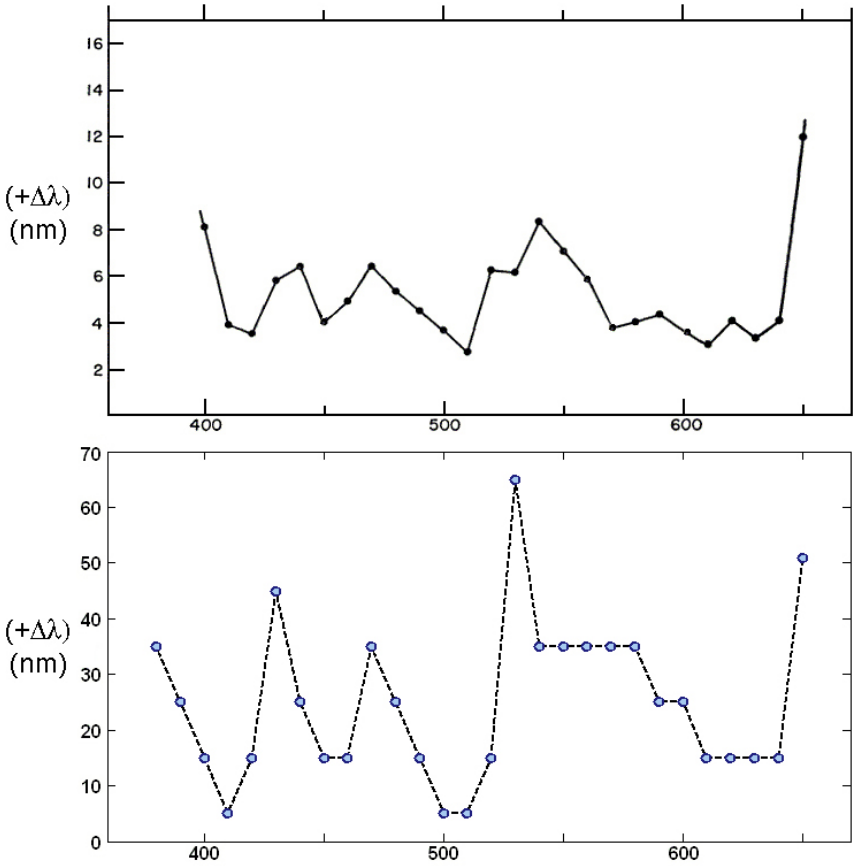

Figure 5.2: Plot of the $(+\Delta\lambda)$ discrimination curve, corresponding to Ingling & Tsou model (bottom) and real data for a single observer and 1.5' visual field (top), adopted from [BW58].

The least noticeable difference towards the longer wavelengths, $(+\Delta\lambda)$, was calculated for each considered λ. Two wavelengths were assumed to differ just noticeably, if the Euclidean distance between the corresponding vectors-responses exceeded a threshold equal to 0.2. The value for the threshold was estimated experimentally.

The results of the described experiment are represented in Figure 5.2, along with the corresponding data from Bedford and Wyszecki [BW58].

It can be seen from Figure 5.2, that although the two curves are not the same, they are actually remarkably alike. The maximum and minimum peaks of both curves fall on approximately the same wavelengths, although the actual magnitude of maximum peaks is several times larger for the prediction of the model than for the real observation data.

5.1.2 Farnsworth-Munsell data set

Munsell color ordering system is based on the principles of color perception. Colors are represented by material standards, embedded in the *Munsell Book of Color*. The colors of the standards are spaced uniformly according to the perception of the observer with normal color vision [WS00].

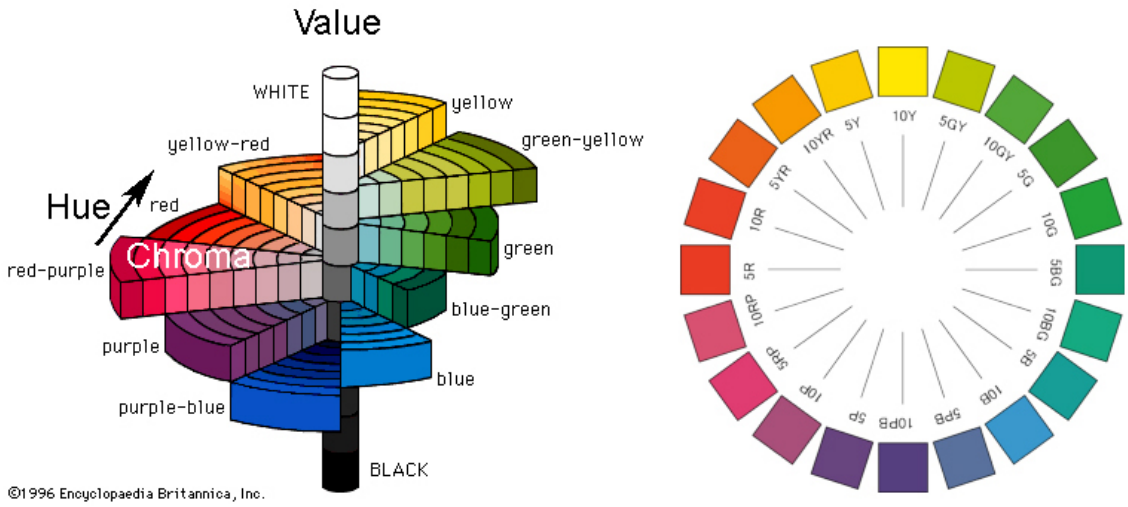

Figure 5.3: Part of the Munsell color cylinder (on the left) and Munsell color circle (on the right).

Each color within the system can be defined in terms of three dimensions: *value*, *hue* and *chroma* (see Fig. 5.3). The value is measured from 0 (black) to 10 (white);

hues form a circle of five principle and five intermediate hues (Purple, Blue, Green, Yellow, Red and PB, BG, GY, YR, RP); chroma represents the "purity" of color (lower chroma - more washed out color) and does not have a maximum, because it varies for different hues and values.

Being based on human visual perception, Munsell color system is often used to evaluate color appearance models. Even though Munsell system is not used directly in this work, however a test set composed of perceptually uniformly distributed color chips is used. It is proposed as well by the Munsell Color Company and is named *Farnsworth-Munsell 100-Hue test*. It is a standard test for defining color vision deficiencies, during which tested subject is asked to arrange about 100 colored chips to form a hue circle, similar to one in Figure 5.3. Based on the difficulties the subject encounters when trying to arrange the chips, it is possible to detect different color vision deficiencies and abnormalities.

In the performed experiment spectral data measured from the Farnsworth-Munsell 100-Hue test set was used. The purpose of this experiment was to demonstrate how the data points will be distributed in the Ingling & Tsou vector space. First, data is transformed to RGB space (Fig. 5.4), taking into account the $D65$ standard illuminant. In RGB space the circular structure of the test hue distribution is apparent. Then the spectral data is transformed to the LMS values using Formula (3.1) on p. 22. Now, using the transformations (4.2) on the page 43, data is transformed to the vector space r-g, y-b, V (Fig. 5.5).

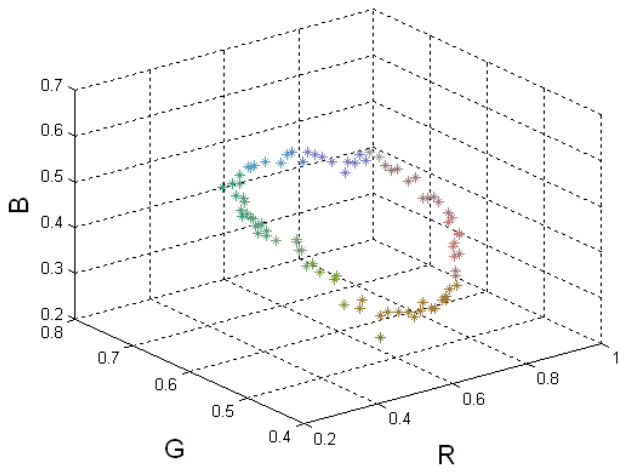

Figure 5.4: The values of the Farnsworth-Munsell 100-Hue test set represented in the RGB space.

From the left part of Fig. 5.5 it may seem that the circular structure of data points

is completely destroyed and order of the points is mixed. However, when changing the view point, the circular organization becomes apparent again (right half of Fig. 5.5). It seems that the order of the hue samples is also preserved. However, this statement requires additional verification which can be an issue for further study.

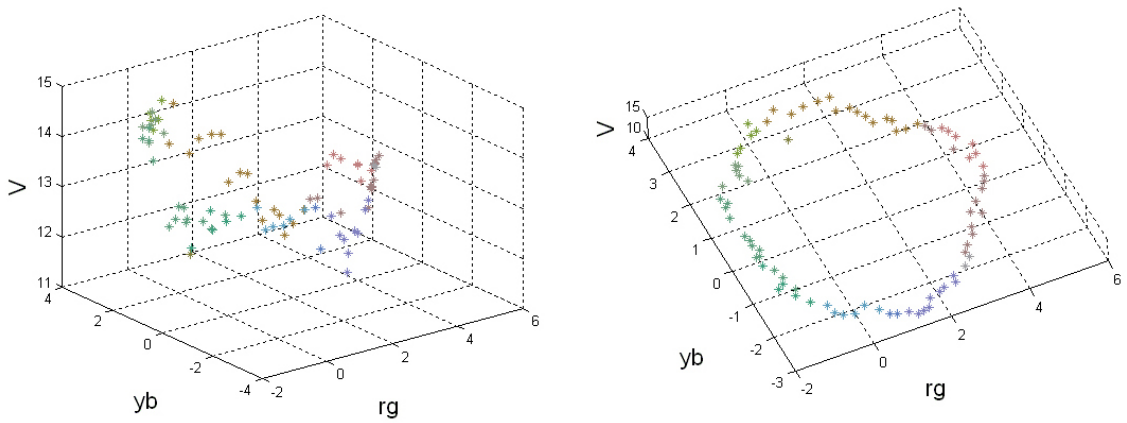

Figure 5.5: The values of the Farnsworth-Munsell 100-Hue test set represented in the r-g, y-b, V space.

5.1.3 Conclusions

In this section two experiments performed with the Ingling & Tsou vector model were described. In both experiments spectral data was used. The experiments were aimed to test both, the vector space organization, and the correspondence of the proposed orthogonal combination with the real human data.

Although, as it was described in this section, the results of the first experiments differ somehow from the human data, those variations may be partly attributed to the differences among observers. It is also possible that there would be some improvements in the results with the variation of the test parameters, such as the threshold and step, which can be a part of further study.

The second experiment showed that proposed transformations preserve the organization of the tested data points. Otherwise, in the case of skewing and packing data points, the discrimination of data points would have been altered and would contradict the real human data.

The described experiments demonstrate the fact, that even a simple two stage model, like the one introduced by Ingling and Tsou, can estimate the outcome

of several vision experiments. Sometimes there is no need for a complex model and simple assumptions are enough.

5.2 Retinex model

The Retinex model for lightness computation has been previously used mainly with the RGB or grayscale images [FCM04, McC99]. This can serve as one of the reasons for possible inaccuracies in the output. In this section different ways of using the Retinex algorithm with the accurate color information, represented by spectral images are proposed. The obtained results are analyzed in the context of color constancy of human vision. Finally, the obtained results are compared with the results of applying Retinex to the RGB images.

One of the considered approaches of applying the Retinex to the spectral images arises from the original idea of Land and McCann [LM71] to process separately the luminance information obtained by the three types of photoreceptors, sensitive to long, middle and short wavelengths (as an analogy to the cone photoreceptors in the retina of human eye). Spectral images provide the accurate color information. By combining it with the information about the light source and the photoreceptor, the accurate photoreceptor responses for each pixel of considered images were obtained (see Equations (2.2) and (3.1) on pages 8 and 22, respectively).

The other suggested approach is the separate Retinex processing of each spectral channel. It is a modification of the previous case in the sense, that here the amount of photoreceptors increases from 3 to the number of spectral channels in the image.

In the performed experiments it was tested how the output of the Retinex algorithm changes for an image when it is examined under different illuminations. As the sources of ambient light, standard illuminants with fixed power distribution were used (Fig. 2.3 on the page 8). Spectral sensitivities of the photoreceptors were obtained from the Stockman and Sharpe (2000) 2° cone fundamentals [SSF99, SS00](Appendix A).

For comparison, L, M and S values were obtained also using a transformation from the original spectra through the CIE XYZ color space given in [WS00]. In addition, the spectral image was transferred to the sRGB and CIELAB spaces [Ber00, WS00]. The Retinex processing was performed independently on the channels of these color spaces.

There are several published versions of the Retinex algorithm. In this work one of the most popular variations of the Retinex algorithm was used. It was suggested by

Frankle and McCann [FM38] and further implemented in MATLAB^{TM} [FCM04]. Further when talking about the Retinex algorithm we will bear in mind the selected implementation.

In order to compare the outputs of applying Retinex to different color representations, the outputs for each representation were converted to the sRGB space using corresponding transformations that can be found in literature [Ber00, WS00]. To display the results with reasonable brightness, the converted images were postprocessed taking into account the response of the output device. The proper modification was obtained experimentally for each image.

Some of the used transformations between color representations can be found in the Appendix B.

We have previously defined (see p. 31) color constancy as a property of human visual system that helps to maintain the color of an object despite the variations in the *illumination conditions* and despite the variations in the *color of the nearby objects*. We use this definition to analyze the performance of the Retinex model. The comparison of the approaches stated above has been done based on two following aspects. First: how well the modeled output preserves the colors of the scene, when varying the spectral power distribution of the ambient light? Second: how the changes in the visible scene affect the color of a specific area of the scene?

As one of the performance measures we suggest to use the *median angular distance* in RGB space. It is a slight modification of commonly used measure for color constancy, when the angle between the RGB of the actual illumination and the RGB of illumination estimate is used [HF04]. For our purposes we considered the same image under different illuminations and compared the Retinex outputs for $D65$ illumination with outputs for other considered illuminations. We calculated the angles between the 3-dimensional vectors (in sRGB space) for every pixel of all tested images and then accepted as a measure the median of all angles for each pair of considered illuminations.

5.2.1 Color constancy (illumination variations)

For the illumination variation experiment 10 different spectral images were used. They were selected to be of different size and wavelength properties. The images were considered under 4 different standard illuminants A, B, C and $D65$ (Fig. 2.3 on the page 8).

Retinex was applied to each considered representation:

- spectra
- L channel of the L*a*b*
- LMS
- sRGB

All outputs were normalized to the interval [0, 1]. The results for all representations were converted to the sRGB space to compare the performance in each case. We calculated the *median angular distance* between the outputs for $D65$ illuminant and for three other illuminants. To summarize the results, we calculated the median and maximum of angular distance for each image and for all cases. Table 5.1 represents the average of those values among 10 tested images (the maximum values represent the maximum over all images).

Table 5.1: Retinex performance for different color representations ("Med" corresponds to the averaged among tested images median angular distance; "Max" is the maximum angular distance over all tested images).

	A to D65		**B to D65**		**C to D65**	
	Med	Max	Med	Max	Med	Max
RGB	6.94	177.3	0.79	168.1	0.19	143.6
L*a*b*	1.10	90	0.48	90	0.13	83.7
LMS	1.51	166.3	0.41	141.0	0.15	62.1
LMS$_{XYZ}$	4.83	164.4	1.24	144.9	0.34	88.6
Spectra	0.00	6.1	0.00	1.5	0.00	0.22

From Table 5.1 we can see that median values for the spectral approach are close to 0.

Although the real reflectance and reflectance estimation of Retinex are not equal, there are considerable similarities between them. We tried to illustrate that in Figure 5.6(a). Left half of it represents the radiance spectra for different illuminants (reflectance multiplied by the light source spectra) for a pixel in one of the tested images. In the right half of the figure we plotted the real reflectance spectra (magenta curve) for the same pixel and the reflectance estimates retrieved with Retinex processing (the same black curve for all illuminants). It can be seen, that the shapes of the curves are quite similar. Nevertheless, it must be pointed out that the similarity is not the case for all pixels of any tested image. Sometimes there also appear some significant deviations from the original reflectance spectrum, as it can be seen from Figure 5.6(b,c).

One can also see from Table 5.1 that differences between results got using L*a*b* values for Retinex input are quite small. This is mostly due to the specifics of the L*a*b* representation itself.

Almost in all cases the results for the RGB are the highest (e.g. the median of 6.94 versus 1.51 for LMS). In the case of LMS space the values are quite small for the median, but the maximum values can be significant. In this case a proper postprocessing is essential.

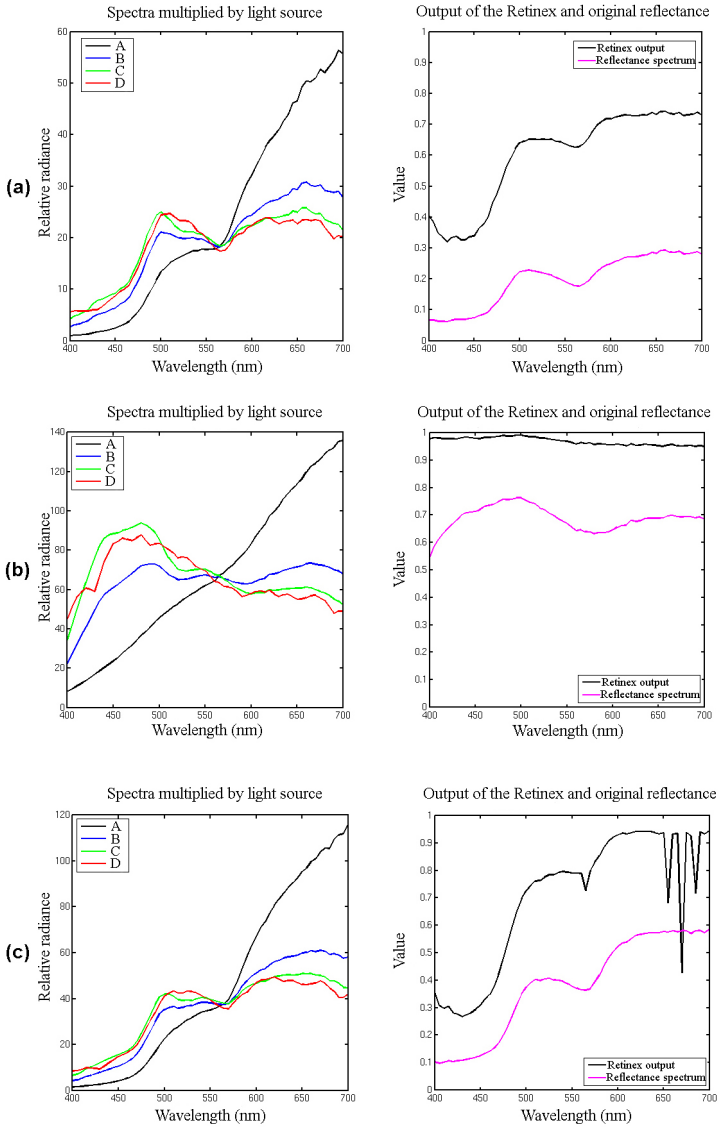

Figure 5.6: The radiance spectra for 4 different illuminations for three different pixels from one of the tested images (on the left) and the original reflectance spectra vs. the estimated by Retinex reflectance of the same pixels (on the right). (a) Retinex estimated reflectance has a similar shape with the real reflectance curve. (b) Retinex output is flatter than the real reflectance curve. (c) Retinex output has the similar shape with the reflectance curve, except the spikes in the area of long wavelengths.

5.2.2 Simultaneous color contrast (scene changes)

For the second part of the evaluation the following vision phenomenon, based on the adaptation mechanism, was used. Let as compare the images from Figure 5.7.

Figure 5.7: sRGB representation of the original spectral image (on the left) and the same image with a cyan filter placed over the yellow square (on the right). As a result the yellow square appears green.

Left image is the sRGB representation of the original spectral image under the $D65$ illumination. On the right image a cyan filter is placed over the yellow square of the same image. As a result it appears green. Now let us apply the same cyan filter to the entire image (Fig. 5.8). Although the actual values for the "yellow" square are exactly the same, as on the right image from Fig. 5.7 (when the filter was placed on the yellow square only and appeared green), we again can recognize the color of the selected square as yellow (although the colors of the whole scene have slightly changed).

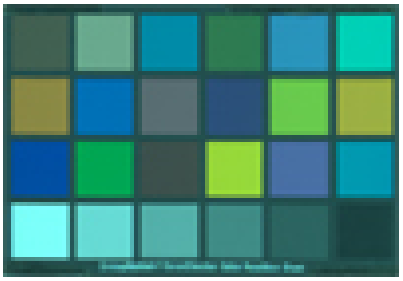

Figure 5.8: A cyan filter is applied to the entire image.

For performing this experiment we modeled the effect of placing a cyan filter over a spectral image (or its part) by eliminating the red component (wavelengths starting from 600 nm) from the spectral power distribution of the ambient light. We used the color checker spectral image and the $D65$ illuminant. As in previous experiment, Retinex was applied to each considered representation (spectra, L* channel of the L*a*b*, LMS, sRGB) of the "filtered" image. The outputs were converted to the

sRGB space to display (after proper normalization to [0, 1]). The desired result after processing would be such that the actual color values of the "yellow" square would shift to green or back to yellow area, depending on whether the filter was applied to the square, or to the whole image.

For comparison the sRGB values of the yellow square are plotted in the sRGB space. In Fig. 5.9 the values for sRGB, L*a*b*, LMS, LMS_{XYZ} and spectra are represented with the filter applied to the yellow square only and to the entire image.

It can be seen, that for L*a*b* and LMS Retinex tends to remove all the illumination without taking into account the real color appearance. The values for the "yellow" square remain mostly the same and are close to yellow (note the differences in scaling of the plots).

In the case of spectra and sRGB the values notably differ and in first case tend to be green, while in the second case (when the filter is applied to the entire image) the values are in the yellow range.

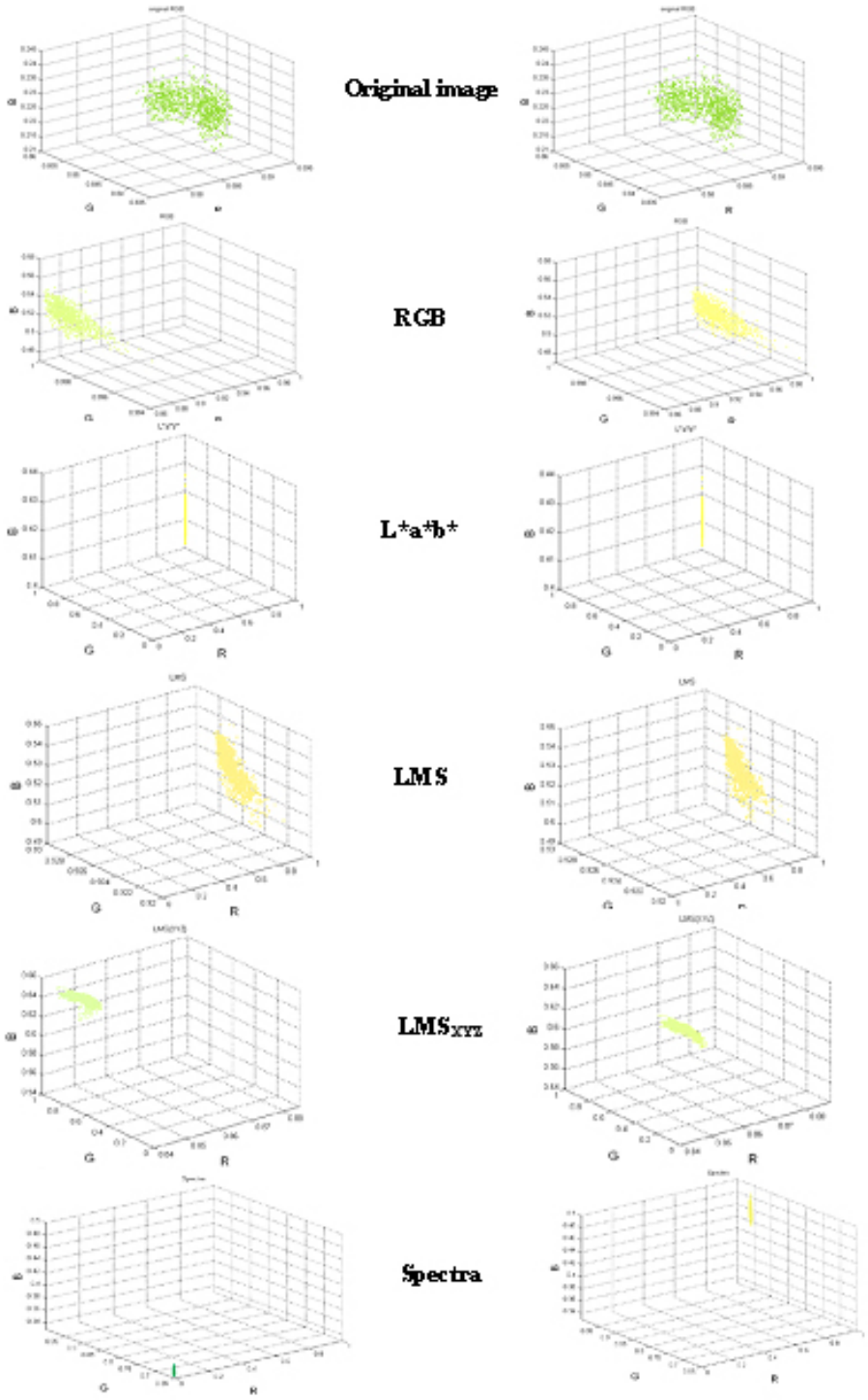

Figure 5.9: The values of the yellow square in the sRGB space. In the left column are the values, when the filter is applied to the square only. In the right column are the values, when the filter is applied to the entire image. Note the scaling differences.

5.2.3 Conclusions

In this section we saw that for different color representations the results differ significantly (Table 5.1 and Fig. 5.9). We noticed that when we apply Retinex to spectral images, the output of the algorithm is in practice always the same independent on the illuminant used for multiplying the original reflectance spectra. To explain this behavior is an interesting topic for our future more detailed research.

In the case of applying Retinex for each spectral channel separately, the algorithm seems to be able to take into account the light source constant by which the reflectance values of each spectral channel are multiplied.

We noted that even though in Figure 5.6(a) the shape of Retinex output and the original reflectance spectrum seem to be quite similar, it is not the case for all spectra in images we have tested (Fig. 5.6(b,c)). This means that there probably does not exist a straightforward way (like scaling by a constant) to map Retinex output directly to reflectance spectra. The postprocessing for spectral Retinex output used in our experiments was just a linear scaling to full [0, 1] range. Because the postprocessing step seems to have quite a large effect on the results, next thing to do is to compare this simple approach with other possibilities for postprocessing.

In general, the output of the Retinex for all color spaces requires a careful selection of the postprocessing method (different for different spaces), which can be a subject of a separate study. The idea of such post Retinex processing can be found in [FM01].

In the second experiment we saw, that Retinex applied to the spectra and RGB space supports the simultaneous color contrast, or changes in the perceived color depending on the surround (see Fig. 5.7, Fig. 5.8 and Fig. 5.9). Although, as it was stated above, the spectral approach needs more complicated postprocessing, the results for it, in the context of this experiment, are closer to human color appearance perception.

Other possible matters for further study are behavior of the algorithm when there are gradual changes of the illumination, and the results of changes in the length of the path and number of paths, which are important parameters of the Retinex algorithm [FM01, CFM04].

Chapter 6

Discussion and Conclusions

Modeling human color vision is a very complex process. It requires a deep understanding of underlying principles and mechanisms, starting with the light signal entering the eye and reaching the retina, and going further through LGN to the primary visual cortex. The main obstacle here is that not all the functions and aspects of human color vision are completely studied and understood yet. In this work we considered some of the known aspects, as well as some mechanisms and theories, and connected them to several existing color vision models.

This work is a part of a large ongoing study, aimed to explore human color vision. One of the goals of this study is to create a sufficient mathematical model of human color vision that will help to study the impact of physiological differences of the human visual system on the color vision. One of such physiological aspects is the spatial distribution of photoreceptors.

It must be pointed out that there is no a superior model of human color vision yet. Thus, a variety of possible improvements and directions of further study can be considered. One of such directions is providing neural zone models with the possibility to predict color appearance. This will lead to the merging of the neural zone and color appearance models into a new, single model type.

Within the limits of this study we concentrated mainly on the Retinex color appearance model. We proposed its application to spectral images and considered different approaches in this direction. We also attempted to evaluate the model and the proposed approaches in the context of human color constancy. The results of the evaluation and the conclusions we drew can be found in the end of Chapter 5, as well as in [PJH+07]. We concentrated on the classical Retinex theory, leaving out numerous variations and modifications, which can probably improve the performance, or change completely the results, described in this work.

The Retinex algorithm itself contains several parameters that can change the performance of the algorithm. Detailed consideration of those parameters is the other possible direction for further study. Finally, a proper postprocessing must be defined to represent the output of the model. To evaluate the results, more methods and tests should be considered.

We also considered a simple neural zone model proposed by Ingling and Tsou. Some tests were designed and carried out to evaluate the performance of this simple model. The results of the experiments along with the corresponding discussion are represented in the end of the first section of Chapter 5.

In general, the comparison and analysis of different models will provide us insight into what really are the essential properties of color vision. One of the possible applications of this knowledge is the spectral imaging. The information about essential vision properties will help to develop new approaches in spectral image analysis and measurements. It would make possible to design applications concentrating only on those aspects that are actually essential for human observers, avoiding redundancy and saving resources.

Appendix A

Cone fundamentals

Cone fundamentals represented here are retrieved from Color & Vision Database [CVR].

A.1 Smith & Pokorny (1975) cone fundamentals

Smith and Pokorny cone fundamentals are obtained from 2° color matching functions [CVR].

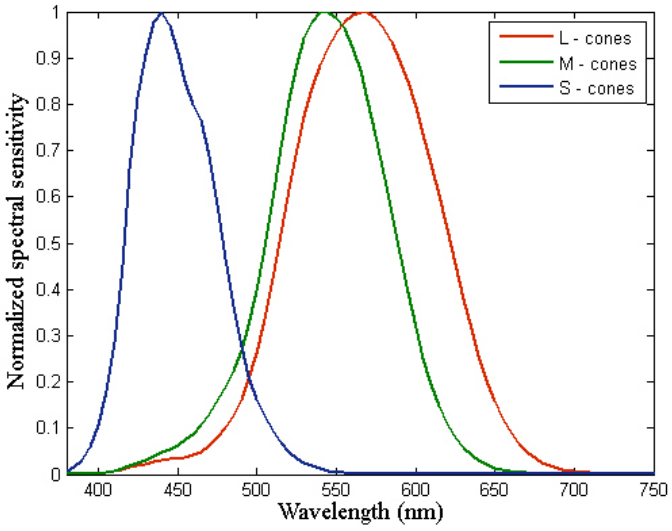

Figure A.1: Cone spectral sensitivities according to Smit and Pokorny [SP75].

Table A.1: Smith & Pokorny (1975) log cone fundamentals: values are tabulated at 5 nm intervals between 380 nm and 825 nm.

Wavelength	**L-cone**	**M-cone**	**S-cone**
380	-3.90984	-4.11396	-4.00788
385	-3.61480	-3.81596	-3.71216
390	-3.31095	-3.50687	-3.40396
395	-3.02732	-3.21710	-3.11803
400	-2.77147	-2.95570	-2.85559
405	-2.55387	-2.72987	-2.63377
410	-2.35744	-2.52161	-2.43311
415	-2.16087	-2.31210	-2.23206
420	-1.99637	-2.12987	-2.06869
425	-1.89531	-2.00212	-1.97757
430	-1.82810	-1.90507	-1.92988
435	-1.76702	-1.81013	-1.89782
440	-1.71715	-1.72773	-1.88776
445	-1.68554	-1.66232	-1.90097
450	-1.66024	-1.60323	-1.92855
455	-1.62991	-1.54253	-1.95838
460	-1.58083	-1.47179	-1.98521
465	-1.50042	-1.38356	-2.00449
470	-1.39875	-1.29200	-2.04956
475	-1.29295	-1.20833	-2.12222
480	-1.18757	-1.13026	-2.21787
485	-1.08708	-1.05536	-2.32817
490	-0.98625	-0.97966	-2.44616
495	-0.88198	-0.89673	-2.56341
500	-0.77600	-0.80829	-2.67416
505	-0.67005	-0.71758	-2.78263
510	-0.56935	-0.63185	-2.90758
515	-0.47987	-0.55775	-3.05822
520	-0.40561	-0.49897	-3.21222
525	-0.34952	-0.45856	-3.34642
530	-0.30741	-0.43267	-3.47972
535	-0.27463	-0.41604	-3.62871
540	-0.24958	-0.40774	-3.79443
545	-0.23059	-0.40676	-3.97212
550	-0.21625	-0.41215	-4.15276
555	-0.20558	-0.42347	-4.32867

Table A.2: Smith & Pokorny (1975) log cone fundamentals (2).

Wavelength	**L-cone**	**M-cone**	**S-cone**
560	-0.19862	-0.44130	-4.48899
565	-0.19575	-0.46655	-4.63073
570	-0.19686	-0.49974	-4.73899
575	-0.20195	-0.54150	-4.80177
580	-0.21140	-0.59287	-4.83951
585	-0.22560	-0.65490	-4.90747
590	-0.24427	-0.72779	-5.00477
595	-0.26725	-0.81145	-5.04804
600	-0.29555	-0.90440	-5.13941
605	-0.32935	-1.00840	-5.25459
610	-0.36944	-1.12007	-5.46406
615	-0.41571	-1.23851	-5.59371
620	-0.47137	-1.36442	-5.68816
625	-0.53932	-1.49957	-5.90105
630	-0.61599	-1.64056	-6.10650
635	-0.69759	-1.78577	-6.25787
640	-0.78674	-1.93588	-6.38739
645	-0.88600	-2.09161	-6.53987
650	-0.99423	-2.24737	-6.71187
655	-1.10970	-2.40114	-6.86810
660	-1.23506	-2.55355	-7.02060
665	-1.37251	-2.71827	-7.18527
670	-1.51310	-2.88096	-7.34813
675	-1.64736	-3.03194	-7.49929
680	-1.78665	-3.18330	-7.65058
685	-1.94229	-3.34646	-7.81361
690	-2.10231	-3.51059	-7.97794
695	-2.25515	-3.66756	-8.13486
700	-2.40345	-3.81748	-8.28501
705	-2.54974	-3.96287	-8.43030
710	-2.69623	-4.10656	-8.57387
715	-2.84583	-4.25204	-8.71937
720	-2.99699	-4.39794	-8.86525
725	-3.14786	-4.54248	-9.00976
730	-3.30144	-4.68916	-9.15631
735	-3.46032	-4.84060	-9.30781

Table A.3: Smith & Pokorny (1975) log cone fundamentals (3).

Wavelength	**L-cone**	**M-cone**	**S-cone**
740	-3.62151	-4.99398	-9.46127
745	-3.78208	-5.14655	-9.61379
750	-3.93956	-5.29555	-9.76284
755	-4.09163	-5.43907	-9.90623
760	-4.24134	-5.58000	-10.04699
765	-4.39206	-5.72142	-10.18856
770	-4.54319	-5.86336	-10.33040
775	-4.69420	-6.00508	-10.47198
780	-4.84542	-6.14674	-10.61374
785	-4.99700	-6.28878	-10.75578
790	-5.14905	-6.43138	-10.89832
795	-5.30167	-6.57451	-11.04145
800	-5.45454	-6.71804	-11.18486
805	-5.60732	-6.86140	-11.32828
810	-5.76007	-7.00485	-11.47169
815	-5.91228	-7.14799	-11.61465
820	-6.06558	-7.29204	-11.75885
825	-6.22236	-7.43988	-11.90671

A.2 Stockman and Sharpe (2000) 2-deg cone fundamentals

Stockman and Sharpe cone fundamentals are obtained from 10° color matching functions, adjusted to 2° [CVR].

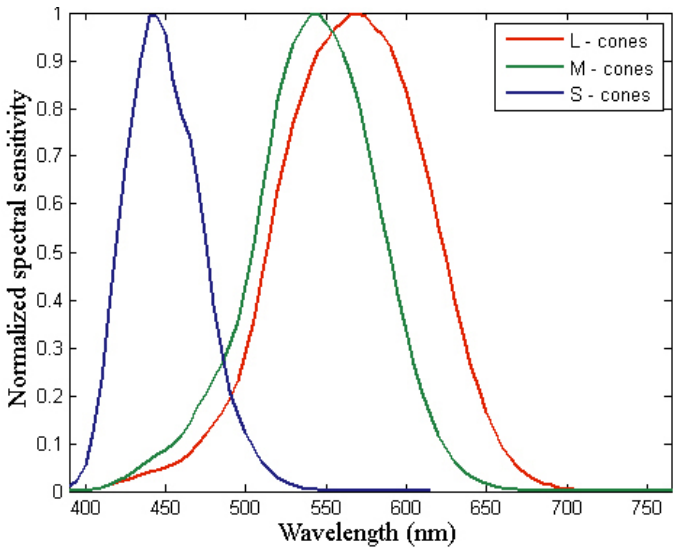

Figure A.2: Cone spectral sensitivities according to Stockman and Sharpe [SS00].

Table A.4: Stockman and Sharpe (2000) 2-deg cone fundamentals: Values are tabulated at 5 nm intervals between 390 nm and 830 nm.

Wavelength	**L-cone**	**M-cone**	**S-cone**
390	4.15003E-04	3.68349E-04	9.54729E-03
395	1.05192E-03	9.58658E-04	2.38250E-02
400	2.40836E-03	2.26991E-03	5.66498E-02
405	4.83339E-03	4.70010E-03	1.22451E-01
410	8.72127E-03	8.79369E-03	2.33008E-01
415	1.33837E-02	1.45277E-02	3.81363E-01
420	1.84480E-02	2.16649E-02	5.43618E-01
425	2.29317E-02	2.95714E-02	6.74474E-01
430	2.81877E-02	3.94566E-02	8.02555E-01
435	3.41054E-02	5.18199E-02	9.03573E-01
440	4.02563E-02	6.47782E-02	9.91020E-01
445	4.49380E-02	7.58812E-02	9.91515E-01
450	4.98639E-02	8.70524E-02	9.55393E-01
455	5.53418E-02	9.81934E-02	8.60240E-01
460	6.47164E-02	1.16272E-01	7.86704E-01
465	8.06894E-02	1.44541E-01	7.38268E-01
470	9.94755E-02	1.75893E-01	6.46359E-01
475	1.18802E-01	2.05398E-01	5.16411E-01
480	1.40145E-01	2.35754E-01	3.90333E-01
485	1.63952E-01	2.68063E-01	2.90322E-01
490	1.91556E-01	3.03630E-01	2.11867E-01
495	2.32926E-01	3.57061E-01	1.60526E-01
500	2.88959E-01	4.27764E-01	1.22839E-01
505	3.59716E-01	5.15587E-01	8.88965E-02
510	4.43683E-01	6.15520E-01	6.08210E-02
515	5.36494E-01	7.19154E-01	4.28123E-02
520	6.28561E-01	8.16610E-01	2.92033E-02
525	7.04720E-01	8.85550E-01	1.93912E-02
530	7.70630E-01	9.35687E-01	1.26013E-02
535	8.25711E-01	9.68858E-01	8.09453E-03
540	8.81011E-01	9.95217E-01	5.08900E-03
545	9.19067E-01	9.97193E-01	3.16893E-03
550	9.40198E-01	9.77193E-01	1.95896E-03
555	9.65733E-01	9.56583E-01	1.20277E-03
560	9.81445E-01	9.17750E-01	7.40174E-04
565	9.94486E-01	8.73205E-01	4.55979E-04

Table A.5: Stockman and Sharpe (2000) 2-deg cone fundamentals (2).

Wavelength	**L-cone**	**M-cone**	**S-cone**
570	9.99993E-01	8.13509E-01	2.81800E-04
575	9.92310E-01	7.40291E-01	1.75039E-04
580	9.69429E-01	6.53274E-01	1.09454E-04
585	9.55602E-01	5.72597E-01	6.89991E-05
590	9.27673E-01	4.92599E-01	4.39024E-05
595	8.85969E-01	4.11246E-01	2.82228E-05
600	8.33982E-01	3.34429E-01	1.83459E-05
605	7.75103E-01	2.64872E-01	1.20667E-05
610	7.05713E-01	2.05273E-01	8.03488E-06
615	6.30773E-01	1.56243E-01	5.41843E-06
620	5.54224E-01	1.16641E-01	
625	4.79941E-01	8.55872E-02	
630	4.00711E-01	6.21120E-02	
635	3.27864E-01	4.44879E-02	
640	2.65784E-01	3.14282E-02	
645	2.13284E-01	2.18037E-02	
650	1.65141E-01	1.54480E-02	
655	1.24749E-01	1.07120E-02	
660	9.30085E-02	7.30255E-03	
665	6.85100E-02	4.97179E-03	
670	4.98661E-02	3.43667E-03	
675	3.58233E-02	2.37617E-03	
680	2.53790E-02	1.63734E-03	
685	1.77201E-02	1.12128E-03	
690	1.21701E-02	7.61051E-04	
695	8.47170E-03	5.25457E-04	
700	5.89749E-03	3.65317E-04	
705	4.09129E-03	2.53417E-04	
710	2.80447E-03	1.74402E-04	
715	1.92058E-03	1.20608E-04	
720	1.32687E-03	8.41716E-05	
725	9.17777E-04	5.89349E-05	
730	6.39373E-04	4.16049E-05	
735	4.46035E-04	2.94354E-05	
740	3.10869E-04	2.08860E-05	
745	2.19329E-04	1.50458E-05	

Table A.6: Stockman and Sharpe (2000) 2-deg cone fundamentals (3).

Wavelength	**L-cone**	**M-cone**	**S-cone**
750	1.54549E-04	1.08200E-05	
755	1.09508E-04	7.82271E-06	
760	7.79912E-05	5.69093E-06	
765	5.56264E-05	4.13998E-06	
770	3.99295E-05	3.02683E-06	
775	2.86163E-05	2.21100E-06	
780	2.07321E-05	1.63433E-06	
785	1.50432E-05	1.21054E-06	
790	1.09446E-05	8.99170E-07	
795	7.97750E-06	6.69594E-07	
800	5.85057E-06	5.03187E-07	
805	4.31102E-06	3.80046E-07	
810	3.17009E-06	2.86329E-07	
815	2.34468E-06	2.16878E-07	
820	1.74666E-06	1.65158E-07	
825	1.30241E-06	1.25508E-07	
830	9.74306E-07	9.53411E-08	

Appendix B

Transformations

Here the transformations between LMS, XYZ and sRGB spaces are represented. More transformations can be found in [Ber00] and [WS00].

XYZ and LMS

The following matrix represents the transition from CIE XYZ color space to the L,M and S cone responses [WS00]:

$$\begin{bmatrix} L \\ M \\ S \end{bmatrix} = \begin{bmatrix} 0.38971 & 0.68898 & 0.07868 \\ -0.22981 & 1.18340 & 0.04641 \\ 0 & 0 & 1 \end{bmatrix} \begin{bmatrix} X \\ Y \\ Z \end{bmatrix}.$$

XYZ and sRGB

The first step in the calculation of sRGB tristimulus values from the CIE XYZ tristimulus values is the following linear transformation, given in [SA96] and [Wik]:

$$\begin{bmatrix} R_1 \\ G_1 \\ B_1 \end{bmatrix} = \begin{bmatrix} 3.2410 & -1.5374 & -0.4986 \\ -0.9692 & 1.8760 & 0.0416 \\ 0.0556 & -0.2040 & 1.0570 \end{bmatrix} \begin{bmatrix} X \\ Y \\ Z \end{bmatrix}.$$

The following formula transforms the linear values R_1, G_1 and B_1 into sRGB. Let

C_1 be R_1, G_1, or B_1, and C_{sRGB} be R_{sRGB}, G_{sRGB}, or B_{sRGB}:

$$C_{sRGB} = \begin{cases} 12.92C_1 & \text{if } C_1 \leq 0.00304 \\ (1+a)C_1^{\frac{1}{2.4}} - a & \text{if } C_1 > 0.00304, \end{cases}$$

where $a = 0.055$.

Bibliography

[Ber00] R.S. Berns. *Billmeyer and Saltzman's principles of color technology*. John Wiley & Sons, New York, 3rd edition, 2000.

[BW58] R.E. Bedford and G.W. Wyszecki. Wavelength discrimination for point sources. *Journal of the Optical Society of America*, 48(2):129, 1958.

[BW86] D.H. Brainard and B.A. Wandell. Analysis of the retinex theory of color vision. *Journal of the Optical Society of America*, 3(10):1651–1661, 1986.

[CFM04] F. Ciurea, B. Funt, and J.J. McCann. Tuning Retinex parameters. *Journal of Electronic Imaging*, 13(1):21–27, 2004.

[CLGP01] P. Capilla, M.J. Luque, J. Gómez, and A. Palomares. On saturation and related parameters following Guth's ATD colour-vision model. *Color research and application*, 26(4):305–321, 2001.

[CMNN00] J. Carroll, C. McMahon, M. Neitz, and J. Neitz. Flickerphotometric electroretinogram estimates of l:m cone photoreceptor ratio in men with photopigment spectra derived from genetics. *Journal of the Optical Society of America*, 17:499–509, 2000.

[CP83] H.D. Crane and T.P. Piantanida. On seeing reddish green and yellowish blue. *Science*, 221(4615):1078–1080, 1983.

[CVR] Color & Vision Database. http://www.cvrl.org/. (Accessed at 2006-2007).

[DVDV93] R.L. De Valois and K.K. De Valois. A multi-stage color model. *Vision Research*, 33(8):1053–1065, 1993.

[Fai98] M.D. Fairchild. *Color Appearance Models*. Addison-Wesley, Reading, Massachusetts, 1998.

[FCM04] B. Funt, F. Ciurea, and J.J. McCann. Retinex in MatLab. *Journal of Electronic Imaging*, 13(1):48–57, 2004.

[FM38] J. Frankle and J.J. McCann. Method and apparatus for lightness imaging. US Patent No. 4,384,336, 1938.

[FM01] B. Funt and J.J. McCann. Control parameters for Retinex. In *Proceedings of the* 9^{th} *Congress of the International Colour Association*, pages 287–290, 2001.

[GS99] K.R. Gegenfurtner and L.T. Sharpe, editors. *Color Vision: From Genes to Perception*. Cambridge University Press, Cambridge, United Kingdom, 1999.

[Gut91] S.L. Guth. Model for color vision and light adaptation. *Journal of the Optical Society of America*, 8(6):976–993, 1991.

[Gut95] S.L. Guth. Further applications of the ATD model for color vision. In *Proceedings of SPIE, The International Society for Optical Engineering*, volume 2414, pages 12–26, 1995.

[Gut98] S.L. Guth. Correcting errors about ATD in Fairchild's "Color Appearance Models". *Color research and application*, 23(5):338–339, 1998.

[HCN+05] H. Hofer, J. Carroll, J. Neitz, M. Neitz, and D.R. Williams. Organization of the human trichromatic cone mosaic. *Journal of Neuroscience*, 25(42):9669–9679, 2005.

[Hel52] H. Helmholtz. Ueber die Theorie der zusammengesetzten Farben. *Annalen der Physik*, 163:45–66, 1852.

[Her64] E. Hering. *Outlines of a Theory of the Light Sense*. Harvard University Press, Cambridge, MA, 1964. Translated by L. Hurvich and D. Jameson.

[HF04] S. Hordley and G. Finlayson. Re-evaluating colour constancy algorithms. In *Proceedings of the* 17^{th} *International Conference on Pattern Recognition*, volume 1, pages 76–79, 2004.

[Ing77] Jr. Ingling, C.R. The spectral sensitivity of the opponent-color channels. *Vision research*, 17:1083–1089, 1977.

[IT77] Jr. Ingling, C.R. and B.H.-P. Tsou. Orthogonal combination of the three visual channels. *Vision research*, 17:1075–1082, 1977.

[JHP+07] T. Jetsu, V. Heikkinen, A. Pogosova, T. Jääskeläinen, and J. Parkkinen. Cone ratio in color vision models. In *Proceedings of the IEEE* 14^{th} *International Conference on Image Analysis and Processing, ICIAP 2007 Workshops*, pages 179–182, Italy, 2007.

[JRW97] D.J. Jobson, Z.U. Rahman, and G.A. Woodell. A multiscale Retinex for bridging the gap between color images and the human observation of scenes. *IEEE Transactions on Image Processing*, 6(7):965–976, 1997.

[Jud51] D.B. Judd. Colorimetry and artificial daylight. In *Proceedings of the CIE*, volume 1, page 11, 1951.

[KB96] P.K. Kaiser and R.M. Boynton. *Human Color Vision (2nd ed.)*. Optical Society of America, Washington, DC, 1996.

[KES+03] R. Kimmel, M. Elad, D. Shaked, R. Keshet, and I. Sobel. A variational framework for Retinex. *International Journal of Computer Vision*, 52(1):7–23, 2003.

[KFN] H. Kolb, E. Fernandez, and R. Nelson. Webvision: The organization of the retina and visual system. http://webvision.med.utah.edu/. (Accessed at 2006-2007).

[Lan62] E.H. Land. Color in natural image. In *Proceedings of the Royal Institution of Great Britain*, volume 39, pages 1–15, 1962.

[Lan83] E.H. Land. Recent advances in retinex theory and some implications for cortical computations: Color vision and the natural image. In *Proceedings of the National Academy of Sciences*, volume 80, pages 5163–5169, 1983.

[Lan86] E.H. Land. An alternative technique for the computation of the designator in the retinex theory of color vision. In *Proceedings of the National Academy of Sciences*, volume 83, pages 3078–3080, 1986.

[LG57] Y. Le Grand. *Light, Colour, and Vision*. John Wiley, New York, 1957.

[LM71] E.H. Land and J.J. McCann. Lightness and Retinex theory. *Journal of the Optical Society of America*, 61(1):1–11, 1971.

[McC99] J.J. McCann. Lessons learned from Mondrians applied to real images and color gamuts. In *Proceedings of IS&T/SID* 7^{th} *Color Imaging Conference*, pages 1–8, 1999.

[McC04] J.J. McCann. Capturing a black cat in shade: past and present of Retinex color appearance models. *Journal of Electronic Imaging*, 13(1):36–47, 2004.

[MPS+98] E. Miyahara, J. Pokorny, V.C. Smith, R. Baron, and E. Baron. Color vision in two observers with highly biased LWS/MWS cone ratios. *Vision Research*, 38(4):601–612, 1998.

[New72] I. Newton. New theory about light and colours. *Philosophical Transactions of the Royal Society*, 6(80):3075–3087, 1672.

[PJH+07] A. Pogosova, T. Jetsu, V. Heikkinen, M. Hauta-Kasari, T. Jääskeläinen, and J. Parkkinen. Spectral images and the Retinex model. In *Proceedings of the* 9^{th} *International Symposium on Multispectral Color Science and Application*, pages 80–85, 2007.

[Ric67] W. Richards. Differences among color normals: Classes I and II. *Journal of the Optical Society of America*, 57:1047–1055, 1967.

[Rob02] D. Roberts. *Signals and Perception: The Fundamentals of Human Sensations*. The Open University, Oxford, United Kingdom, 2002.

[RW99] A. Roorda and D.R. Williams. The arrangement of the three cone classes in the living human eye. *Nature*, 397(6719):520–522, 1999.

[SA96] M. Stokes and M. Anderson. A standard default color space for the Internet - sRGB. http://www.w3.org/Graphics/Color/sRGB, November 5 1996. (Accessed on 19 October 2006).

[SP75] V.C. Smith and J. Pokorny. Spectral sensitivity of the foveal cone photopigments between 400 and 500 nm. *Vision Research*, 15(2):161–171, 1975.

[SS00] A. Stockman and L.T. Sharpe. Spectral sensitivities of the Middle- and Long-wavelength sensitive cones derived from measurements in observers of known genotype. *Vision Research*, 40:1711–1737, 2000.

[SSF99] A. Stockman, L.T. Sharpe, and C.C. Fach. The spectral sensitivity of the human short-wavelength cones. *Vision Research*, 39:2901–2927, 1999.

[Vos78] J.J. Vos. Colorimetric and photometric properties of a 2 degree fundamental observer. *Color research and application*, 3:125–128, 1978.

[WGRB90] H. Wassle, U. Grunert, J. Rohrenbeck, and B.B. Boycott. Retinal ganglion cell density and cortical magnification factor in the primate. *Vision Research*, 30(11):1897–1911, 1990.

[Wik] sRGB. http://en.wikipedia.org/wiki/Srgb. (accessed on 19 October 2006).

[WS00] G.W. Wyszecki and W.S. Stiles. *Color Science: Concepts and Methods, Quantitative Data and Formulae (2nd ed.)*. Wiley-InterScience, 2000.

[XF06] W. Xiong and B. Funt. Stereo retinex. In *Proceedings of the The 3^{rd} Canadian Conference on Computer and Robot Vision (CRV'06)*, page 15, 2006.

[You02] Th. Young. On the theory of light and colours. *Philosophical Transactions of the Royal Society of London*, 92:12–48, 1802.